Effect of dikes on saltwater intrusion under various wind conditions in the Changjiang Estuary

Linjiang Li[1], Jianrong Zhu[1], Robert J Chant[2], Chuning Wang[2], L. Fernando Pareja-Roman[3]

[1]State Key Laboratory of Estuarine and Coastal Research, East China Normal University, Shanghai, 200062, PR China

[2]Department of Marine and Coastal Sciences, Rutgers University, New Brunswick, New Jersey, USA

[3]Department of Civil, Environmental, and Ocean Engineering, Stevens Institute of Technology, Hoboken, New Jersey, USA.

Corresponding author: Jianrong Zhu (jrzhu@sklec.ecnu.edu.cn); Linjiang Li (li_linjiang@126.com)

Key Points:

- Water level rise on the north side of dikes strengthens the counterclockwise horizontal circulation under strong north wind
- Dikes decrease saltwater intrusion in the North Channel under climatic wind but increase it under strong north wind
- Under strong north wind, mixing in the North Channel decreases with the saltwater intrusion increase due to the implementation of dikes

Abstract

To improve navigation, the Deep Waterway Project (DWP) was implemented in the north passage of the Changjiang Estuary in 1998, and consists of a deep channel protected by two dikes. By altering estuarine morphology, the DWP can affect saltwater intrusion and mixing, with implications for drinking water intake and supply. In this study, we employ a numerical model to study the influence of dikes on saltwater intrusion in the estuary under climatic and persistent, strong northerly wind conditions that occurred in February 2014. Model results show that the dikes prevent the southward transport of relatively low-salinity water at the mouth of the North Channel (NC) under climatic wind conditions, resulting in the weakening of saltwater intrusion and mixing in this channel. Under persistent strong northerly wind conditions, relatively high-salinity water is transported southward to the mouth of the NC and blocked by the dikes, causing a water level rise at the mouth of the NC. As a result, a large amount of high-salinity water is advected into the NC and then out to the sea through the South Chanel, forming a counterclockwise horizontal circulation. Overall, the DWP favors water intake at the reservoir in the NC under climatic wind conditions and is unfavorable under persistent strong northerly winds (>9 m/s), which can lead to extremely severe saltwater intrusion.

Plain Language Summary

Coastal engineering projects such as channel deepening and dike installation can affect saltwater intrusion in estuaries, and the response may also be modulated by winds. In this paper, we used a numerical model to explore the impact of the dikes of the Deep Waterway Project (DWP) on saltwater intrusion in the Changjiang Estuary under various wind conditions. Under climatic winds, water in the North Channel (NC) of the estuary is relatively fresh due to the high river discharge. Lateral dikes prevent the southward transport of relatively diluted, low salinity water at the mouth of the NC, resulting in an accumulation of diluted water and the weakening of saltwater intrusion and mixing in the NC. Under strong northerly winds, salinity in the NC increases abnormally due to the southward transport of high-salinity water. Dikes block the southward salt transport and increase the landward water and salt transport into the NC. Although salinity increased in the NC with the implementation of the dikes, the salinity variance and mixing decreased. The influence of dikes on salt intrusion and mixing in the Changjiang under climatic winds is different to that under strong northerly winds.

1. Introduction

Major coastal cities of the world are located near estuaries due to the ease of access to transportation and recreation. Maritime transportation typically requires the construction of channels, ports, and other structures to minimize navigational hazards. Such human interventions can significantly alter basin morphology and have a great impact on tides (Chant et al., 2018), flooding (Ralston et al., 2019) and saltwater intrusion (C. Liu et al., 2019; Lyu & Zhu, 2018b). The impact on saltwater intrusion is crucial for urban estuaries, as it can affect the drinking water supply for large populations. Some coastal cities are experiencing increased risk of low water quality due to projects that alter estuarine morphology. For example, channel deepening increased the saltwater intrusion in the Hudson River Estuary and affected the drinking water supply of New York City (Ralston & Geyer, 2019). Shifts in saltwater intrusion can also alter estuarine circulation through adjustments in salinity gradients (Geyer & MacCready, 2014; Hansen & Rattray, 1965; Pritchard, 1956) and mixing (X. Li et al., 2018; P. MacCready et al., 2018; Wang et al., 2017). For example, C.

Liu et al. (2019) found that land reclamation has decreased landward salt transport, which has weakened mixing in the Pearl River Estuary. While previous studies have reported how coastal structures can alter salt intrusion in estuaries, few consider the response to various wind conditions even though it has been reported that winds can also contribute. For example, Zhang et al. (2019) reported that the frequency of saltwater intrusion events in the Changjiang Estuary is increasing in recent years due to the increasing frequency of winter storms passing the East China Sea. In this section, we describe the dynamics of saltwater intrusion and its relation to winds and then introduce the case of saltwater intrusion in the Changjiang Estuary.

1.1 Dynamics of Saltwater Intrusion

Saltwater intrusion in the estuaries is determined by the competition of many physical processes. River discharge tends to drive salt out of the estuary while tidal dispersion and baroclinic flows tend to move salt upstream through a process that resembles Fickian diffusion (Monismith et al., 2002). In steady-state, the extent of saltwater intrusion is proportional to the cross-sectional area and depth of the estuary, and inversely proportional to river discharge and tidal current amplitude. This steady-state theory approximately describes salinity dynamics in estuaries such as the Hudson River Estuary (Lerczak et al., 2006) and Pearl River Estuary (Gong & Shen, 2011).

The wind is another factor affecting the saltwater intrusion. For example, wind-driven sea-level setups at the mouth of estuaries can produce landward flows that outcompete river runoff, resulting in the net, landward advection of salt (Aristizabal & Chant, 2015). Along-estuary winds can also strain density gradients, and the associated destruction or enhancement of stratification depend on wind direction, the Wedderburn number, and the entrainment depth ratio (Chen & Sanford, 2009). In multi-inlet coastal systems, the residual horizontal circulation can be influenced by winds and can alter salt transport through each inlet. Examples include the Dutch Wadden Sea (Duran-Matute et al., 2014; Duran‐Matute et al., 2016), the Ria Formosa (south of Portugal) multi-inlet lagoon (Fabião et al., 2016), the Altamaha River Estuary (C. Li, 2013) and Venice lagoon (Bellafiore et al., 2008). While the effect of winds on saltwater intrusion and circulation has been studied in other cases, relatively little is known about the role of wind on saltwater intrusion in estuaries where morphology has been significantly modified through the construction of shipping channels and other structures. The goal of this paper is to explore wind-driven saltwater intrusion in highly urbanized estuaries. The study region considered here is the Changjiang Estuary, China, whose present-day landscape significantly differs from natural, pre-development conditions. We use a numerical model to explore the response of the salt field to climatic wind conditions and under relatively strong, northerly wind events typical of the winter season. We discuss how the salt field responds to differences in wind forcing, and how these responses are modulated by multiple estuarine branching and coastal dikes.

1.2 The Changjiang Estuary

The Changjiang (Yangtze River) Estuary is a large, multi-branch estuary (Figure 1). Chongming Island divides the estuary into the North and South Branches. The South Branch is further divided by Changxing Island into two channels, the North Channel (NC) and South Channel (SC). The SC is divided by the Jiuduan Sandbank into two passages, the North and South Passages. The Changjiang Estuary is adjacent to Shanghai, an international metropolis, and a maritime shipping center for China. Prior to harbor engineering works, sand bars at the river mouth prevented large ships from traveling through. To meet demands of maritime transportation, the Deep Waterway Project (DWP) was implemented in the North Passage of the Changjiang Estuary in 1998. The DWP included the construction of two dikes: the north dike, which is 49.2 km long, and the south dike, which is 48 km long. In addition, a waterway approximately 300 m wide was dredged from approximately 7 m to 12.5 m deep at the center of the North Passage (G. Liu et al., 2011; Zhu et al., 2006). The dikes, which are ~0.37 m higher than mean sea level, are submerged during high tides and exposed during low tides. The Qingcaosha Reservoir was constructed in the upper reaches of the NC and supplies approximately 5.5 million cubic meters of water to Shanghai every day, accounting for 70% of the water consumption in the city. This reservoir is a vital water resource for Shanghai that is often adversely affected by saltwater intrusion during the dry (winter) season (L. Li et al., 2014; Qiu & Zhu, 2013; Qiu et al., 2012; Wu et al., 2006). When the salinity at reservoir water intakes (labeled 'QCS1' in Figure 1) exceeds 0.45 psu (the salinity standard for drinking water), the intakes shut down to prevent saline water flushes into the reservoir.

Previous studies have demonstrated that saltwater intrusion into the North Branch and NC increases during the dry season when northerly winds prevail (L. Li et al., 2012; Wu et al., 2010). On the other hand, Zhu et al. (2006) noted that the dikes of the DWP prevent the southward transport of diluted water from the NC. Wu et al. (2010) found that the dikes prevent the transport of high-salinity water from the South Passage over the shoals and into the NC. The consensus is that the dikes mitigate saltwater intrusion in the NC and tend to maintain suitable salinity values at the Qingcaosha Reservoir. However, both studies are based on climatic wind conditions and do not consider the response to episodic wind events. In February 2014, strong and persistent northerly winds drove a severe saltwater intrusion event in the NC; a maximum salinity of 9 psu was observed at reservoir water intakes. This event provides an opportunity to quantitatively determine the role of dikes of the DWP in saltwater intrusion under strong winds. The relevance of this study is twofold: first, results herein will help inform environmental management practices both in Shanghai and in other urban estuaries of the world where wind events can significantly impact saltwater intrusion. Second, we offer insight into the role of coastal engineering projects on fundamental estuarine dynamics. This article is organized as follows: Section 2 introduces the numerical model and experimental design; section 3 contains the results of the numerical experiments; section 4 presents the discussion; and section 5 lists the conclusions.

2. Methods

2.1 Numerical Model and Experimental Design

The semi-implicit Estuarine, Coastal, and Ocean Model (ECOM-si) was used in this study (Blumberg, 1994). This model has been improved and validated many times in this system, e.g., as discussed in Wu and Zhu (2010) and Lyu and Zhu (2018a). Monthly mean wind data with a temporal resolution of 6 h from the National Centers for Environmental Prediction/Quick Scatterometer (NCEP/QSCAT) dataset was used. A persistent, strong northerly wind event occurred in the Changjiang Estuary and its adjacent sea from February 7^{th} to 14^{th}, 2014 (Figure 2). During this event, the weather station on the east shoal of Chongming Island (labeled as 'WS' in Figure 1) measured a maximum wind speed of 15 m/s. The wind field in the model domain was simulated at a spatial resolution of 0.005°×0.005° using output from the Weather Research and Forecast (WRF) model. The modeled wind speed and direction agree well with observations. To evaluate error, the wind vector is decomposed into meridional and zonal components. The correlation coefficients (r^2, defined in appendix A) for meridional and zonal components are 0.62 and 0.67, respectively. The model skill scores (SS, defined in appendix A) for meridional and zonal components are 0.77

and 0.64, respectively. Time series of river discharge for the model correspond to measurements at the Datong hydrological station. The monthly mean river discharge in February 2014 was 10800 m^3/s, close to the mean value of 11,500 m^3/s for February. The open ocean boundaries were provided by tidal levels and residual water levels. Tidal levels were calculated by combining the harmonic constants of the 16 main tidal constituents. Residual water levels, including those under climatic wind conditions and the persistent strong wind in February 2014, were calculated using the results of a numerical model over a larger domain that includes the Bohai, Yellow, and East China Seas (Wu et al., 2011). Further details on model boundaries and initial conditions are provided by Lyu and Zhu (2018b). Model bathymetry corresponds to depth soundings collected in 2014. The model was run from January 1st to February 28th 2014, and the results from February 6th to 28th were analyzed.

Two sets of numerical experiments were designed to compare the effects of climatic winds and persistent strong northerly winds in February 2014. In each set of the experiments, two scenarios (with and without DWP dikes) were considered. A total of four numerical experiments were performed.

2.2 Analytical Methods

2.2.1 Transport and Salt Fluxes

To compute horizontal and cross-sectionally integrated water transport fluxes, the water transport per unit width is defined as follows:

$$\vec{Tr} = \frac{1}{T}\int_0^T \int_{-1}^0 (h+\xi)\vec{V}\, d\sigma dt \quad (1)$$

where h is the water depth, ξ is the water level, $\vec{V}$ is the water velocity vector, T is the averaging period, and σ is the relative depth (0 at the surface and -1 at the bottom). The net, cross-sectionally integrated water flux is:

$$F_q = \left\langle \iint u dA \right\rangle = \left\langle \int_0^L \int_{-1}^0 (h+\xi) u d\sigma dy \right\rangle \quad (2)$$

where $\langle\ \rangle$ represents time averaging (i.e. a 36 h low-pass filter), A is the tidally-varying cross-sectional area and dA its differential, L is the channel width, and u is the current velocity perpendicular to the cross-section.

The net, cross-sectionally integrated salt flux is given by:

$$F_s = \left\langle \iint uS dA \right\rangle = \left\langle \int_0^L \int_{-1}^0 (h+\xi) uS d\sigma dy \right\rangle \quad (3)$$

where S is the salinity. To better understand the mechanism of salt flux transport in the Changjiang Estuary, the current velocity was decomposed as follows (Lerczak et al., 2006):

$$u_0(t) = \frac{1}{A_0}\left\langle \iint u(y,\sigma,t) dA \right\rangle = \frac{1}{A_0}\left\langle \int_0^L \int_{-1}^0 (h+\xi) u d\sigma dy \right\rangle \quad (4)$$

$$u_e(y,\sigma,t) = \frac{\langle udA \rangle}{\langle dA \rangle} - u_0(t) \quad (5)$$

$$u_t(y,\sigma,t) = u - u_e(y,\sigma,t) - u_0(t) \quad (6)$$

where A_0 is the low-passed cross-sectional area. The first term, u_0, represents the spatially and temporally averaged current velocity. The second term, u_e, represents the temporally averaged current velocity, which changes spatially and reflects the vertical structure of the flow caused by baroclinity. The third term, u_t, is the tidal current, which changes spatially and temporally. Salinity can also be decomposed into three terms. Thus, the cross-sectionally integrated salt flux is decomposed as:

$$
\begin{aligned}
F_s &= \left\langle \int_0^L \int_{-1}^0 (h+\xi) uS d\sigma dy \right\rangle \\
&= \left\langle \int_0^L \int_{-1}^0 (h+\xi)(u_0+u_e+u_t)(S_0+S_e+S_t) d\sigma dy \right\rangle \\
&= \left\langle \int_0^L \int_{-1}^0 (h+\xi)(u_0 S_0+u_e S_e+u_t S_t + cross\ terms) d\sigma dy \right\rangle \quad (7) \\
&\approx \left\langle \int_0^L \int_{-1}^0 (h+\xi)(u_0 S_0+u_e S_e+u_t S_t) d\sigma dy \right\rangle \\
&= Q_0 S_0 + F_e + F_t
\end{aligned}
$$

$Q_0 S_0$ is the advective salt flux and represents the flux due to river discharge or meteorological-induced flows. F_e is the steady shear salt flux caused by estuarine circulation. F_t is the tidal oscillatory salt flux owing to temporal correlations between u and S. The cross terms are generally small and can be neglected in this analysis (Lerczak et al. 2006).

2.2.2 Derivation of the mixing relation using salinity variance and TEF frameworks

In the ocean turbulence community, the mixing of a tracer is defined by the tracer variance dissipation rate (Osborn & Cox, 1972; Stern, 1968). Saltwater intrusion changes the salinity variance and mixing in the channel. Considering a three-dimensional domain (e.g. an entire estuary), we can decompose the salinity as $S = \bar{S} + S'$ where the overbar denotes the volume average and a prime denotes the total deviation from the volume average. The salinity variance can then be defined as $S'^2 = (S - \bar{S})^2$. It is possible to derive a salinity variance budget equation based on algebraic manipulation of the Reynolds-averaged advection–diffusion equation for salinity:

$$\frac{\partial S}{\partial t} = -U \bullet \nabla S + K\nabla^2 S \quad (8)$$

where U is the three-dimensional velocity vector and K is the diffusivity tensor. Multiplying (8) by $2S'$ we get the evolution of the salinity variance:

$$\frac{\partial (S'^2)}{\partial t} + U\nabla(S'^2) = \nabla \bullet (2KS'\nabla S') - 2K(\nabla S')^2 - 2S'\frac{\partial \bar{S}}{\partial t} \quad (9)$$

Taking the integral of (9) over an estuarine volume with open boundaries, we get the variance budget:

$$\frac{d}{dt}\int S'^2 dV = -\int u_n S'^2 dA_{open} - 2\int K(\nabla S')^2 dV \quad (10)$$

where u_n is the outward-normal velocity on the open boundaries with area A_{open}.Thus, the rate of change of the net salinity variance (term on the left) is governed by only two terms: the advective inputs of the variance at the open boundaries (first term on the right) and the loss of the variance due to turbulent mixing (second term on the right).

Now we describe the TEF (Total Exchange Flow) framework by MacCready (2011). At any cross section in the channel we define:

$$Q_{in} = \left\langle \int_{A^+} u dA \right\rangle, Q_{out} = \left\langle \int_{A^-} u dA \right\rangle \quad (11)$$

$$S_{in} = \frac{\left\langle \int_{A^+} uSdA \right\rangle}{Q_{in}}, S_{out} = \frac{\left\langle \int_{A^-} uSdA \right\rangle}{Q_{out}} \quad (12)$$

A^+ and A^- denote the regions of the cross-section where water enters or leaves the domain, respectively. In (11) and (12), Q_{in}, S_{in}, Q_{out}, S_{out} are the Total Exchange Flow (TEF) terms. The sum $Q_{in} + Q_{out}$ is the net water transport driven by river discharge or wind, and $Q_{in}S_{in} + Q_{out}S_{out}$ is the net salt transport.

MacCready et al. (2018) expressed the TEF framework in terms of the the salinity variance. Following this concept, we explore the salinity variance TEF terms and mixing in a box-type estuary with two boundary sections: Lower and Upper boundary (Figure 4). By take the tidal average of (10) with the advection terms decomposed using the TEF analysis method, we find the tidally-averaged salinity variance balance in TEF terminology:

$$\frac{d}{dt}\left\langle \int S'^2 dV \right\rangle = [Q_{in}(S'^2)_{in} + Q_{out}(S'^2)_{out})]\big|_{Lower} + [Q_{in}(S'^2)_{in} + Q_{out}(S'^2)_{out}]\big|_{Upper} - M$$

(13)

where

$$(S'^2)_{in} = \frac{\left\langle \int_{A^+} (S - \bar{S})^2 udA \right\rangle}{Q_{in}}; (S'^2)_{out} = \frac{\left\langle \int_{A^-} (S - \bar{S})^2 udA \right\rangle}{Q_{out}} \quad (14)$$

and $M = 2\left\langle \int K(\nabla S')^2 dV \right\rangle$ represents the volume-integrated rate of destruction of salinity variance.

3. Results

3.1 Salinity Response under Climatic Wind Conditions

In this part, we analyze the response of salinity to climatic (February) wind forcing in scenarios that include and exclude the dikes of the DWP. As shown in Figure 5 (left panel), the implementation of the dikes led to a decrease in salinity in the North Channel. The reduced mean salinity values at the Baozhen (BZ), Qingcaosha reservoir intakes (QCS1), and lower Qingcaosha (QCS2) stations are 0.39, 0.04, and 0.47 psu, respectively. The maximum salinity values at these locations are, in the same order, 3, 0.7, and 2.5 psu. These results indicate that the dikes of the DWP cause a significant decrease in saltwater intrusion in the NC under climatic wind conditions, which favors the intake of water in the Qingcaosha Reservoir. The latter is consistent with previous findings (Wu et al., 2010; Zhu et al., 2006). In contrast, there is a significant increase in saltwater intrusion in the SC with the implementation of the DWP (Figure 5, right panel). The mean increases in salinity at Pudong Airport (PD), Hengsha (HS), and Changxing (CXD) stations are 1.77, 2.33, and 0.74 psu, respectively. The maximum salinity values at these three stations are 4, 5 and 3 psu, in the same order.

The horizontal distribution of averaged salinity is shown in Figure 6. With the DWP and during neap tides, salinity at reservoir intakes is below 0.45 psu (Figure 6a), and therefore the water is suitable for further treatment. On average, salinity in the SC is higher than in the NC, a discrepancy that is attributed to stronger landward Stokes transport generated by tides in the South Passage (Wu et al., 2010). Landward Stokes transport pushes seawater upstream and prevents freshwater from entering the SC through the fork. During spring tides, the transport is even greater and more low-salinity water is diverted into the NC (Figure 6b). To better quantify the residual circulation, the water diversion ratio (defined in Appendix B) is used to determine the proportion of freshwater entering the NC at the fork. Specifically, the water diversion ratio in the NC is 0.40 averaged over neaps, 0.58 over springs, and 0.53 over a full spring-neap cycle. Note that the 0.45 psu isohaline during spring tides is an exception and does not follow the general salinity distribution (Figure 6b). This slightly saline water mass may spill from the North Branch and then be advected seaward through the NC and SC, creating a reversal in the along channel salinity gradient (Lyu & Zhu, 2018a; Wu et al., 2006; Xue et al., 2009) .

Without the implementation of the DWP (in Figure 6c and Figure 6d the dashed lines denote the dikes, indicating only the location of the DWP), saltwater intrusion strengthens in the NC and weakens in the SC during both neap and spring tides. The horizontal distribution of salinity differences without and with the implementation of the DWP shows that the salinity in the NC decreases during neap tide and reaches more than 5 psu in the sand bar area with the implementation of the DWP. Also note a small salinity change at the water intake of the Qingcaosha Reservoir. The salinity increases in the SC and has a maximum value of more than 6 psu around the Jiuduan Sandbank. Changes in salinity patterns during spring tide are similar to those during neap tide. With the implementation of the DWP, it can be seen that the north dike blocks the southward transport of relatively low-salinity water from the NC, resulting in an accumulation of diluted water and a decrease in salinity in the NC. In the South Passage, the topography changed into a funnel shape with the implementation of the DWP, which strengthens the saltwater intrusion (Wu et al., 2010). Meanwhile, the southward transport of relatively low-salinity diluted water from the NC is blocked, which also caused the increase in salinity in the South Passage.

The influences of the DWP on saltwater intrusion in the NC are greatly weakened when the southward transport of diluted water is blocked by the north dike. Figure 7 shows the water and salt fluxes in a cross-section along the north dike with and without the implementation of the DWP. Without the DWP, the volume transport is southward during neap tides and northward during spring tides. This is primarily because water transport is largely induced by northerly winds during neap tides and by tidal transport during spring tides. During neap tides, the wind-driven southward transport surpasses northward tidal transport. The opposite conditions occur during spring tides (Wu et al., 2018; Wu et al., 2010). During neap tides, the southward transport of water was approximately 4,200 m^3/s without the implementation of the DWP, but essentially disappeared with the implementation of the DWP. This is because water transport is blocked by the dikes, as the tidal range is small during neap tides (less than 2.5 m) and the dikes are 0.37 m higher than the mean sea level. These results are consistent with Zhu et al. (2006). As demonstrated in Figure 7c, during neap tides the southward salt flux is only approximately 20 t/s without the implementation of the DWP because the southward transported water is relatively low-salinity. The salt flux nearly vanishes (~0 t/s) with the implementation of the DWP.

During spring tides, the dikes block the tidal transport over tidal flats from the South Passage to the NC, and the northward water flux decreases from approximately 10,000 m^3/s without the implementation of the DWP to less than 5,000 m^3/s with the implementation of the DWP. The change in the overtopping water flux results in a change in the salt flux. During spring tides, the South Passage is occupied by high-salinity water and the dikes effectively weaken the transport of high-salinity water from south to north. The northward salt flux transport decreases from a maximum of 215 t/s to 75 t/s (Figure 7c), thereby resulting in a decrease in salinity in the NC. These results are consistent with those of Wu et al. (2010). Figure 8a shows the changes in the water fluxes across the section in the NC (sec1 in Figure 1). Due to the river discharge, the cross-sectionally integrated water flux (Equation (2)) is seaward regardless of whether the DWP is implemented. However, there is a difference in the magnitude with and without the implementation of the DWP. During neap tides (February 9th to 14th), there is a decrease in the seaward water flux with the implementation of the DWP because the original southward transport from the NC is blocked by the north dike, resulting in an increase in the water level and a decrease in the seaward discharge of water in the NC. During spring tides (February 15th to 18th), there is an increase in the seaward water transport in the NC because the South Passage has a large tidal prism and the original water transport across the tidal flats from south to north is blocked by the dikes, resulting in a decrease in the water level at the mouth of the NC. Consequently, the downstream discharge of water from the SC into the South Passage is blocked and the water diversion ratio in the NC increases (L. Li et al., 2010).

Figure 8b shows the changes in salt fluxes across the section in the NC. During the neap tide, the landward salt flux decreased in contradiction with decreasing seaward water flux. The cause of this phenomenon was noted above. With the implementation of the DWP, low-salinity water is retained in the NC, resulting in a reduction of the landward salt flux in the NC. These results are consistent with those of Zhu et al. (2006). During the spring tide (February 15th to 17th), the seaward salt flux slightly increases. This is because the increasing seaward water flux in the spring tide carries salts that have entered the NC during the neap tide outside the river mouth. Regardless of whether the DWP is present, through this cross-section, a salt flux enters the NC during the neap tide and exits the NC during the spring tide. This process is important for maintaining the estuarine salt balance. The salt flux decomposition (Figures 8c and d) shows that, during neap tide, the landward steady shear transport is relatively strong due to weak tidal stirring. The strong landward steady shear transport combined with the landward tidal transport surpasses the seaward advective salt flux. As a result, the net salt flux is landward during neap tides. During spring tides, the landward steady shear transport weakens as a result of intense stirring and is insufficient to compensate the seaward advective transport. As a result, salt is transported seaward. Overall, we find that the mechanisms of estuarine salt transport under climatic wind conditions are the same regardless of the modeled scenario (with and without DWP).

3.2 Salinity Response under Strong Northerly Winds

Now we consider the response of the circulation and salt transport under strong northerly winds. Time series of salinity at stations without and with the DWP are shown in Figure 9. With the DWP, there is an increase in salinity in the NC. The mean salinity values at the BZ, QCS1, and QCS2 stations are 1.31, 0.65 and 1.12 psu, and the maximum values are, 6, 5.5 and 6 psu, respectively. These results suggest that saltwater intrusion in the NC under sustained northerly winds results in unfavorable conditions for drinking water intake at the reservoir. The salinity values at the three observation stations in the SC decrease in the scenario with the DWP. The reduced mean salinities at the PD, HS, and CXD stations are 0.62, 3.39 and 1.70 psu, respectively, while the reduced maximum salinities are 4, 15 and 9 psu, respectively. This suggests that the saltwater intrusion into the SC weakens under strong northerly wind conditions with the DWP. In addition to the model results, we present a time series of observed salinity during strong wind conditions and found SS for these stations are higher than 0.7 (Figure 8). The latter provides additional confirmation that the numerical model used in this study can accurately simulate the processes that lead to saltwater intrusion in the Changjiang Estuary.

Residual water levels and transport (Equation 1) with and without the DWP are shown in Figure 10, and correspond to an average during neap conditions (February 10th to

13th). Under strong northerly winds, water is transported from north to south along the coast. The net transport of water in the NC is landward due to landward Ekman transport, which overcomes runoff and downstream flow. The direction of water transport changes at the bifurcation of the NC and the SC. Water flows into the SC and then flows downstream into the South and North Passages, forming a horizontal circulation pattern. The north dike of the DWP blocks the southward wind-driven current, which then flows eastward along the north dike. There is a rise in the residual water levels on the north side of the dike due to its blocking action. Without the DWP, water transport induced by persistent strong northerly winds is directly southward in the sand bar region and no rise in the residual water levels occurs. Consequently, the horizontal circulation initiated by strong winds and characterized by landward water transport in the NC and seaward water transport in the SC is considerably weaker. Specifically, the maximum landward water transport per unit width decreases by more than 2 m^2/s in the NC and the maximum seaward transport per unit width decreases by more than 2 m^2/s in the SC (Figure 10e) without the implementation of the DWP. The spatial distribution of differences in the residual water levels with and without the implementation of the DWP shows that residual water levels on the north side significantly increase, as much as 10 cm, due to the blockage of the north dike, whereas water levels over a large area significantly decrease, as much as 10 cm, in the South Passage.

The right panel of Figure 10 shows the distribution of the vertically averaged salinities with and without the implementation of the DWP and their differences during the neap tide from February 10th to 13th. As a result of the landward transport of water in the NC under the aforementioned strong northerly winds, extremely severe saltwater intrusion occurs in the NC. The entire NC is occupied by high-salinity water (Figure 10b and 10d) . With the implementation of the DWP, the average salinity at the water intake location of the Qingcaosha Reservoir exceeds 5 psu and saltwater enters the SC from the NC at their point of bifurcation. Severe saltwater intrusion occurs in the SC and the North and South Passages, but to a far lesser extent than saltwater intrusion in the NC. These results are opposite to those calculated under climatic wind conditions. Without the implementation of the DWP, saltwater intrusion will weaken in the NC but strengthen in the SC. The distribution of the differences in salinity without and with the implementation of the DWP shows that the blockage of the north dike results in a greater than 4 psu increase in salinity in the NC and a greater than 5 psu decrease in salinity in the SC under persistent northerly wind conditions.

As a result of the horizontal transport of water caused by persistent northerly winds, which flows landward in the NC and seaward in the SC, peak salinity occurs earlier in the NC than in the SC as the high-salinity water is transported from north to south. As Figure 9 shows, peak salinities occur on approximately February 12th at stations in the NC, whereas peak salinities occur by February 17th at stations in the SC. Without the dikes, water is transported southward (Figure 10c), resulting in a rapid increase in salinity at the HS and CXD stations in the SC (red line on the right side of Figure 9). As a result, the peak salinity phase occurs earlier at these locations, on approximately February 13th.

The model results of water fluxes also reveal that the dikes lead to a counterclockwise circulation pattern with landward flow in the NC and seaward in the SC. By quantifying the cross-sectionally integrated water flux, the amount of water blocked by the north dike and the amount of water that flows upstream in the NC are presented as follows. As shown by the temporal variations in the water and salt fluxes in a cross-section along the north dike (Figure 11), without the implementation of the DWP, a large amount of water crosses the section from the NC into the South Passage during the neap tide and under the strongest northerly winds from February 7th to 14th . The instantaneous maximum water flux reaches 2.8×10^4 m^3/s on February 10th, which is more than six times the flux that occurs under climatic wind conditions. The salt flux in a cross-section along the dike is also large. Its maximum value is up to 730 t/s; however, under climatic wind conditions, it is less than 25 t/s (Figure 7c). With the implementation of the DWP, the water flux and corresponding salt flux through the cross-section are both approximately 0 due to the blockage by the north dike. Southerly winds occurred during the spring tide on February 16th . Due to tidal transport and the southerly winds, both the water and salt fluxes are transported from south to north and are significantly greater without the implementation of the DWP than with the implementation of the DWP.

With the implementation of the DWP, the water flux across the section in the NC is transported landward from February 8th to 13th and has a maximum of 11,000 m^3/s under the persistent, strong northerly wind conditions, which approaches the river discharge of the same period (Figure 12a). However, without the implementation of the DWP, the landward water flux is less than 1,500 m^3/s. The landward water volume transport increases by nearly an order of magnitude with the implementation of the DWP. This occurs because of the sea-level set-up associated with blockage of the southerly flows by the DWP. Stated differently, a sea-level setup at the mouth of the NC and produces a landward pressure gradient. The cross-sectionally integrated salt flux demonstrates that regardless of whether the DWP is implemented, salt is transported landward during strong northerly winds that occurred from February 7th to 14th (Figure 12b). However, there is a significant difference in salt flux with and without the implementation of the DWP. The maximum salt flux entering the NC reaches 260 t/s with the implementation of the DWP and is less than 150 t/s without the implementation of the DWP. During southerly wind and spring tide conditions on February 15th , regardless of whether the DWP is present, salt begins to be transported to the open sea and the intensity of the seaward salt transport is higher if the DWP is present. The aforementioned results of the temporal variations in the salinity at the observation stations, the horizontal distribution of the salinities and the changes observed without and with the implementation of the DWP are consistent with the conclusion that changes in saltwater intrusion are induced by changes in water and salt fluxes in the NC. Temporal variations in the decomposed salt flux terms show that, from February 9th to 14th and with the implementation of the DWP, large advective transport plays a dominant role in landward salt transport while steady shear and tidal transport play a comparatively insignificant role (Figure 12c). Without the implementation of the DWP, steady shear transport dominates the landward salt transport mechanism, whereas advective transport plays an insignificant role (Figure 12d) and results in weakened salt transport when the DWP is absent.

Table 1 summarizes the dominant mechanisms of landward salt flux across the section at the mouth of NC from February 9th to 13th in each experiment. Under climatic wind conditions, regardless of whether the DWP is implemented, steady shear transport caused by the estuarine circulation controls the landward salt transport. Tidal transport is not strong through this cross-section. Under the observed, persistent strong northerly wind conditions, a large amount of water is transported by advection into the NC by Ekman transport, bringing a large amount of salt into the NC due to the implementation of the DWP. As a result, an extremely severe saltwater intrusion occurs.

To maintain a water balance, after a large amount of ocean water flows into the NC, the ocean water is discharged downstream into the sea through the SC (Figure 10a). Time series of water flux across the section in the SC (sec2) show that under climatic wind conditions, with the DWP present, the water flux increases during neap tide and decreases during spring tides, but the differences between the fluxes is insignificant and approximately half of the river discharge measured at the Datong station (Figure 13). Driven by the observed wind in February 2014, there is a significant difference in the water flux in the SC. With the DWP present, the peak seaward water flux reaches 20,000 m^3/s, which is roughly twice that as without the DWP and is also approximately twice the actual river discharge. The peak water flux occurs on February 10, when there is a strong northerly wind and a neap tide. With the implementation of the DWP, the enhanced seaward water flux in the SC pushes the isohaline downstream in the SC (Figure 10b and Figure 10d), thereby decreasing the saltwater intrusion in the SC.

3.3 Salinity Variance Budget and Mixing

In this section, the mixing in the NC is quantitatively determined using salinity variance. The domain of NC is defined as a box with two open boundaries (lower and upper sections in Figure 1). Under climatic wind conditions, the peak mixing (Equation 13) is 1.21 $\times 10^6$ psu^{2}m^3 s^{-1} without the DWP and 7.35$\times 10^5$ psu^{2}m^3 s^{-1} with the DWP. This discrepancy is mainly from the landward advection of salinity variance (the first term on the right of Equation 13, which is determined by the difference between the salinity at the boundary section and volume-averaged salinity, and the water fluxes at the boundary) into the NC (Figure14c and 14d). Salinity variance fluxes through the upper boundary (the second term on the right of Equation 13) are also greater in the scenario without the DWP (Figure 14e and 14f). On the other hand, regardless of whether the DWP is implemented, peak mixing occurs during the transition from neap to spring tides when the strong deviation encounters strong turbulence. The timing of peak mixing is similar to that of an idealized estuary in P. MacCready et al. (2018) as well as the Hudson Estuary (Wang & Geyer, 2018).

The flux-weighted salinity variances in the TEF framework (Equation 14), volume-averaged salinity and volume-averaged salinity variance $\left\langle V^{-1}\int S'^2 dV \right\rangle$ under the climatic wind conditions are shown in Figure 15. Without the implementation of the DWP, the flux-weighted salinity variances at both boundaries increase. The increase at the lower boundary is due to the increase in landward salt flux; the increase at the upper boundary is caused by the increase of volume-averaged salinity in the NC. As shown in Figure 15e and 15f, the maximum volume-averaged salinity is ~ 4 psu with the implementation of the DWP and increases to ~6 psu without DWP. Meanwhile, the maximum volume-averaged salinity variance is ~ 18 psu^2 with DWP, which increases to ~25 psu^2 without DWP. Overall, without the implementation of DWP, both the salinity variance and mixing increase in the NC.

On the other hand, under strong northerly winds, the peak mixing is 1.6$\times 10^6$ psu^{2}m^{3}s^{-1} and 2.3$\times 10^6$ psu^{2}m^3 s^{-1} with and without the implementation of DWP, respectively (Figure 16a). Interestingly, the salt fluxes across sec1 decrease without DWP (Figure 12b), whereas the salinity variance fluxes increase. Model results show that flux-weighted salinity variances at the lower and upper sections decrease with the implementation of the DWP (Figure 17a, b, c, and d). The maximum volume-averaged salinity is ~17.5 psu and ~14.3 psu with and without the implementation of the DWP, respectively; meanwhile, the maximum volume-averaged salinity variance is ~ 40 psu^2 and ~ 53 psu^2 with and without the implementation of the DWP, respectively (Figure 17e and 17f).

Under climatic wind conditions, the mixing increases with the increase of saltwater intrusion in the NC. On contrary, under persistent strong northerly wind conditions of February 2014, the mixing decreases with the increase in saltwater intrusion in the NC. Overall, mixing in NC is much stronger under strong north wind as a result of wind stirring and landward Ekman transport regardless of whether the DWP is implemented.

4. Discussion

4.1 Seasonal variability

The river discharge and winds in the Changjiang Estuary display pronounced seasonal variability. During the winter season, the river discharge is relatively low, with the lowest climatic discharge about 11500 m^3/s in January and February. The highest discharge occurs in July (mean 50000 m^3/s) (Figure 18a). The northerly winter monsoon (speed of 6-7 m/s) typically dominates in December, January and February (Figure 18b). The southerly summer monsoon is relatively strong in July, with a wind speed of approximately 4.3 m/s (Figure 18b). To assess the seasonal changes in salinity, the model was run for one year using the climatic winds and discharge with seasonal variations as Figure 18a and 18b show. To examine the influence of DWP, two scenarios were considered: one with the DWP and the other without the DWP. The results show that the salinities at QCS1 are highest in January and February regardless of whether the DWP is implemented. During the wet season (from May 1st to Nov 1st), the salinity at QCS1 and salt flux at the mouth of NC are 0 due to strong river discharge and weak northerly winds. The observed salinity at BZ from 2010 to 2018 (Figure 18e) evidences the pronounced seasonal variability that higher salinity occurs in the winter season and lower salinity occurs in the summer season.

The salinity at QCS1 decreases with the implementation of the DWP under the climatic discharge and winds. Specifically, the reduced mean salinities at the QCS1 in December, January and February are 0.02,0.08 and 0.04 psu, respectively (Table 2). The reduced maximum salinities at the QCS1 in December, January and February are 0.29, 0.96 and 0.47 psu, respectively (Table 2). This salinity difference becomes weak from March and then disappears due to increasing river discharge and deceasing winter monsoon. The implementation of the DWP decreases the number of days that the Qingcaosha Reservoir could not use water from the Changjiang (salinity at QCS1 exceeding 0.45 psu) in January, February, and March under the climatic discharge and winds. Specifically, the number of reduced days is 3.86, 2.9 and 0.12 day, respectively (Table 2). The landward salt flux across sec1 first occurs in December with the implementation of the DWP, however, it first occurs in November without the implementation of the DWP. From December to February, salt fluxes across sec1 display pronounced spring-neap variation regardless of whether the DWP is implemented. However, without the implementation, the maximum landward salt fluxes across sec1 increase 13.89, 10.4 and 14.98 t/s in December, January and Feb, respectively (Table 2).The salt flux across sec1 is always seaward in March due to increasing discharge and weakening of north winds regardless of whether the DWP is implemented. Overall, the seaward shift in salinity in the NC (based on the landward slat flux across sec1, but similarly for other sections in the NC) due to dike installation has been modest compared with the monthly-to-seasonal variability due to tides, river discharge and monsoon.

4.2 Sensitivity Analysis on Wind Speed

Most of the saltwater intrusion events in the Changjiang Estuary occur during the winter season (Figure 18e). Northerly winds prevail in the Changjiang Estuary in winter, but wind statistics have not been analyzed. In this section we use the wind observations at the WS station (for the location, see Figure 1) in winter (December, January and Feb) from 2005 to 2019 to briefly show the frequency of wind near the research cite (Figure 19). It is evident that northerly winds of 4-10 m/s dominate in winter, with an average wind speed of approximately 6.4 m/s. If strong wind is defined as wind speed exceeding 9 m/s, the frequency of strong wind period is about 14% during the winter season. To assess the influence of the DWP on saltwater intrusion under various wind speeds in winter, we carry out numerical experiments with different north wind speeds occurring from February 8 at 0:00. Here, 8 sets of wind speeds from 2 m/s to 16 m/s with an increment of 2 m/s are considered. At each wind speed set, two scenarios were considered: one with the DWP and the other without the DWP.

At low wind speeds (≤8 m/s), the volume-averaged salinity of the NC increased compared to the implementing case (Figure 20, right panel). At high wind speeds (≥10 m/s), the reverse was true, as the volume-averaged salinity of the NC decreased compared to the implementing case (Figure 20, right panel). The critical wind speed for the DWP to switch role in saltwater intrusion is about 9 m/s (Figure 20i). As wind speed increases, the response time of salinity to DWP dikes becomes shorter (Figure 20, black triangles); at 10 m/s it takes 2.7 days for salinity to diverge (dS>0.2 psu) while at 16 m/s it only takes 0.75 day.

4.3 Comparison to other studies

Wind-induced horizontal circulation in the Changjiang Estuary has been reported in previous studies. Wu et al. (2010) concluded that when discharge and tides are excluded, the pure wind-driven unit width water transport is about 2 m^2/s landward in the NC and seaward in the SC under a northerly wind at 7 m/s; L. Li et al. (2012) reported the pure wind-driven unit width water transport increases to about 4 m^2/s under the a northerly wind at 10 m/s. In this study, we note the dikes of DWP have a strong effect on the wind-induced horizontal circulation. Without the implement of the DWP, the landward unit width water transport in the NC deceases about 2 m^2/s under the strong, northerly wind conditions of February 2014.

Zhu et al. (2006) reported that the dikes of the DWP block the southward drift of freshwater driven by the northerly monsoon;Wu et al. (2010) reported that the dikes of the DWP block the northward drift of saline water in the South Passage invading into the and NC through tide-induced transport. In this study, the water and salt fluxes across the north dike are quantified (Figure 7 and Figure 11). In addition, we find that salinity in the NC decreased with DWP under the climatic wind, which is consistent with Zhu et al. (2006) and Wu et al. (2010); under strong north wind (>9 m/s), however, the conclusion reverses and salinity in the NC increases due to the dikes blocking the southward drift of high-salinity water. Results show that the orientation of the dikes relative to the mean offshore current is a significant factor affecting salinity in the NC.

We now place our results in context with other estuaries. Y. Yang and Chui (2018) evaluated the independent and combined effects of wind regime and land reclamation projects on the circulation at Mai Po Tidal Marsh in the Deep Bay, Pearl River Estuary. It is discovered that the reclamation projects in the bay enhance the effects of southwest monsoon in accelerating estuarine circulation during the summer season, but inhibit the effects of northeast monsoon decelerating estuarine circulation during the winter season. In addition, the reclamation projects in the bay lowered the bay's average salinity for both seasons. In this study, we find dikes can have opposite influence on salinity in the NC depending on northerly wind speed in winter. While in summer, the salinity in the NC is constantly low due to southerly wind and higher discharge, regardless of whether the DWP is present (Figure 18). Z. Yang and Wang (2015) found the loss of intertidal flats due to human interventions results in an increase in saltwater intrusion and stronger mixing in the in Whidbey Basin of Puget Sound. However, the effect of wind was not consider in that study. In this study, we find the DWP decreases the saltwater intrusion and mixing in the NC under climatic wind in winter; under the strong, northerly wind conditions of February 2014, the saltwater intrusion increases but mixing decreases in the NC with the implement of the DWP. Based on this finding, we suggest studying the effects of estuarine constructions on mixing in other estuaries under various wind conditions.

4.4 Future works in the Changjiang Estuary

The competition between wind straining and gravitational circulation modifies stratification and mixing in estuaries, but its impact in the Changjiang Estuary has not been discussed. Previously the Wedderburn number (Chen & Sanford, 2009) is used to assess the role of wind on the tilting of isohalines in an idealized estuary; however, in Changjiang Estuary the north wind is not aligned with the main axis of the channel. In such case, the lateral Wedderburn number (Purkiani et al., 2016) may be a better criterion to evaluate the contribution of wind straining, which can be applied in the Changjiang Estuary.

Under the influence of ongoing climate change, many estuaries and coastal regions are exposed to increasing extreme climate events. In the Changjiang Estuary, Zhang et al. (2019) reported that the frequency of winter storm and salinity in the North Branch increased from 1994 to 2008. How this trend contributes to saltwater intrusion in the NC and SC should be investigated since our study suggests that DWP could enhance saltwater intrusion during winter storms.

5. Conclusions

In this study, the influences of the DWP on saltwater intrusion in the NC of Changjiang Estuary under climatic wind conditions and persistent northerly wind conditions that occurred in February 2014 are simulated using a three-dimensional numerical saltwater intrusion model. The results show that under climatic wind conditions, the north dike of the DWP blocks the southward transport of relatively low-salinity diluted water in the NC, resulting in an accumulation of diluted water as well as the weakening of saltwater intrusion in the NC and the strengthening of saltwater intrusion in the SC. During neap tides, the water and salt fluxes in a cross-section along the north dike are transported from the NC to the South Passage by the northerly wind without the implementation of the DWP and essentially disappear with the implementation of the DWP due to blockage by the north dike. During spring tides, the higher salt water is moved by tidal transport from the South Passage to the NC if the DWP is absent and the amount of salt water decreases significantly if the DWP is present. The implementation of the DWP results in a decrease in the seaward water flux cross section in the NC during neap tide and an increase in this water flux during spring tides, and a decrease in the landward salt flux during neap tide and a slight increase in the seaward salt flux.

Under the persistent strong northerly wind conditions of February 2014, the southward alongshore transport of water occurred outside the Changjiang Estuary. As a result of the wind-driven Ekman transport, water was transported upstream from the sea into the NC and changed direction at the bifurcation between the NC and SC, then flowed downstream in the SC, forming a horizontal circulation. If the DWP is present, this horizontal circulation strengthens significantly, resulting in the maximum unit width net water transport increasing by 2 m^2/s. The blockage by the north dike leads to a significant increase in the residual water levels on the northern side of the north dike. During neap tide, extremely severe saltwater intrusion occurs in the NC; the salinity at the water intake of the Qingcaosha Reservoir increases by as much as 5.5 psu, whereas the salinity in the SC significantly decreases. The water and salt fluxes in the cross-section along the north dike are transported southward in large amounts without the implementation of the DWP, but tend to 0 with the implementation of the DWP. The water flux across the section in the NC is transported landward during neap tide with the implementation of the DWP and this flux is approximately equal to the river discharge; the flux is greater than eight times that without the implementation of the DWP. Regardless of whether the DWP is implemented, the salt flux is transported landward under strong northerly winds, but with the implementation of the DWP, the salt flux is significantly greater than (1.7 times) without the DWP. Based on the salt flux decomposition, the advective transport plays a dominant role in the landward salt transport with the implementation of the DWP, whereas the steady shear transport plays a dominant role without the implementation of the DWP. Under climatic wind conditions, the DWP is favorable to the water intake of the Qingcaosha Reservoir; however, the DWP can cause severe saltwater intrusion in the NC under persistent strong northerly wind conditions, which is unfavorable to the water intake of the Qingcaosha Reservoir. This should merit the attention of reservoir management authorities.

Saltwater intrusion causes a change in salinity deviation both along and cross channel thus changing the mixing in the channel. Under climatic wind conditions, salinity in NC is lower compared with that under strong northerly wind conditions, and the implementation of DWP decreases saltwater intrusion as well as mixing. Under strong north wind, the NC is occupied by high salinity water; the implement of the DWP increased the saltwater intrusion but decreased the salinity variance and mixing in the NC. Since mixing primarily occurs in vertical direction, a decomposition of salinity variance in horizontal and vertical direction could help to better identify and quantify mixing in the system (X. Li et al., 2018). For example, under the strong northerly wind condition, without the presence of DWP, landward salt flux is dominated by the estuarine flux and more vertical variance is generated and then consumed by mixing in the estuary. On contrary, with the presence of DWP, landward salt flux is dominated by advective flux, and less mixing is generated in the estuary due to lack of vertical variance. In future works, we strongly suggest to perform similar analysis in other estuaries with artificial engineering projects, as such intervention may enhance or inhibit saltwater intrusion under different weather conditions.

Appendix A: Model Validation

The correlation coefficient (r^2) and skill score (SS) were used to evaluate the model results against the observed data as follows (Conroy et al., 2019; Lyu & Zhu, 2018a; Qiu & Zhu, 2013):

$$r^2 = \frac{\sum (X_{\mathrm{mod}} - \overline{X}_{\mathrm{mod}})(X_{obs} - \overline{X}_{obs})}{[\sum (X_{\mathrm{mod}} - \overline{X}_{\mathrm{mod}})^2 \sum (X_{obs} - \overline{X}_{obs})^2]^{1/2}} \quad \text{(A1)}$$

$$SS = 1 - \frac{\sum \left|X_{\mathrm{mod}} - X_{obs}\right|^2}{\sum (\left|X_{\mathrm{mod}} - \overline{X}_{obs}\right| + \left|X_{obs} - \overline{X}_{obs}\right|)^2} \quad \text{(A2)}$$

where X_{mod} is the modeled data, X_{obs} is the observed data, and $\overline{X}$ is the mean value.

Appendix B: Water diversion ratio

The water diversion ratio is the proportion of freshwater transported from headwaters to each branch of the estuary. Two transects, the upper section and sec2 in Figure 1, are used to calculate the water diversion ratio in the North and South channels. The water diversion ratio in the North channel is calculated as follows:

$$R = \frac{(Q_{in} + Q_{out})\big|_{Upper}}{(Q_{in} + Q_{out})\big|_{Upper} + (Q_{in} + Q_{out})\big|_{\sec 2}} \quad \text{(B1)}$$

The water diversion ratio in the South Channel is then $1 - R$. When R =1, all of the river water discharges into the sea through the North Channel, while R =0 indicates that none of the river water discharges into the sea through the channel. R <0 indicates landward flux across the lower section, which can be caused by severe coastal storms.

Acknowledgments

This work was supported by the China Scholarship Council and the National Natural Science Foundation of China (41676083), Shanghai Institute of Eco-Chongming. L. Fernando Pareja-Roman was supported by the U.S. National Science Foundation, Prediction of and Resilience to Extreme Events (PREEVENTS) program. All data sets used in this study are publicly available at https://figshare.com/s/21e3d13d23605209af75

References

Aristizabal, M. F., & Chant, R. J. (2015). An observational study of salt fluxes in Delaware Bay. *Journal of Geophysical Research-Oceans, 120*(4), 2751-2768. <Go to ISI>://WOS:000354417200021

Bellafiore, D., Umgiesser, G., & Cucco, A. (2008). Modeling the water exchanges between the Venice Lagoon and the Adriatic Sea. *Ocean Dynamics, 58*(5-6), 397-413.

Blumberg, A. (1994). A primer for ECOM-si. *Technical report of HydroQual*, 66.

Chant, R. J., Sommerfield, C. K., & Talke, S. A. (2018). Impact of channel deepening on tidal and gravitational circulation in a highly engineered estuarine basin. *Estuaries and Coasts, 41*(6), 1587-1600.

Chen, S.-N., & Sanford, L. P. (2009). Axial wind effects on stratification and longitudinal salt transport in an idealized, partially mixed estuary. *Journal of Physical Oceanography, 39*(8), 1905-1920.

Conroy, T., Sutherland, D. A., & Ralston, D. K. (2019). Estuarine exchange flow variability in a seasonal, segmented estuary. *Journal of Physical Oceanography*.

Duran-Matute, M., Gerkema, T., De Boer, G., Nauw, J., & Gräwe, U. (2014). Residual circulation and freshwater transport in the Dutch Wadden Sea: a numerical modelling study. *Ocean Science, 10*(4), 611-632.

Duran-Matute, M., Gerkema, T., & Sassi, M. G. (2016). Quantifying the residual volume transport through a multiple-inlet system in response to wind forcing: The case of the western Dutch Wadden Sea. *Journal of Geophysical Research: Oceans, 121*(12), 8888-8903.

Fabião, J. P. F., Rodrigues, M. F. G., Fortunato, A. B., de Brito Jacob, J. M. Q., & Cravo, A. M. F. (2016). Water exchanges between a multi-inlet lagoon and the ocean: the role of forcing mechanisms. *Ocean Dynamics, 66*(2), 173-194.

Geyer, W. R., & MacCready, P. (2014). The estuarine circulation. *Annual review of fluid mechanics, 46*, 175-197.

Gong, W., & Shen, J. (2011). The response of salt intrusion to changes in river discharge and tidal mixing during the dry season in the Modaomen Estuary, China. *Continental Shelf Research, 31*(7-8), 769-788.

Hansen, D. V., & Rattray, M. (1965). Gravitational circulation in straits and estuaries. *Journal of Marine Research, 23*, 104-122.

Lerczak, J. A., Geyer, W. R., & Chant, R. J. (2006). Mechanisms driving the time-dependent salt flux in a partially stratified estuary. *Journal of Physical Oceanography, 36*(12), 2296-2311. <Go to ISI>://WOS:000243206300006

Li, C. (2013). Subtidal water flux through a multiple-inlet system: Observations before and during a cold front event and numerical experiments. *Journal of Geophysical Research: Oceans, 118*(4), 1877-1892.

Li, L., Zhu, J., & Wu, H. (2012). Impacts of wind stress on saltwater intrusion in the Yangtze Estuary. *Science China-Earth Sciences, 55*(7), 1178-1192. <Go to ISI>://WOS:000305891900012

Li, L., Zhu, J., Wu, H., & Guo, Z. (2014). Lateral Saltwater Intrusion in the North Channel of the Changjiang Estuary. *Estuaries and Coasts, 37*(1), 36-55. <Go to ISI>://WOS:000330588000003

Li, L., Zhu, J., Wu, H., & Wang, B. (2010). A numerical study on water diversion ratio of the Changjiang (Yangtze) estuary in dry season. *Chinese Journal of Oceanology and Limnology, 28*(3), 700-712. <Go to ISI>://WOS:000278924100034

Li, X., Geyer, W. R., Zhu, J., & Wu, H. (2018). The Transformation of Salinity Variance: A New Approach to Quantifying the Influence of Straining and Mixing on Estuarine Stratification. *Journal of Physical Oceanography, 48*(3), 607-623.

Liu, C., Yu, M., Jia, L., Cai, H., & Chen, X. (2019). Impacts of physical alterations on salt transport during the dry season in the Modaomen Estuary, Pearl River Delta, China. *Estuarine, Coastal and Shelf Science, 227*, 106345.

Liu, G., Zhu, J., Wang, Y., Wu, H., & Wu, J. (2011). Tripod measured residual currents and sediment flux: Impacts on the silting of the Deepwater Navigation Channel in the Changjiang Estuary. *Estuarine, Coastal and Shelf Science, 93*(3), 192-201.

Lyu, H., & Zhu, J. (2018a). Impact of the bottom drag coefficient on saltwater intrusion in the extremely shallow estuary. *Journal of Hydrology, 557*, 838-850.

Lyu, H., & Zhu, J. (2018b). Impacts of Tidal Flat Reclamation on Saltwater Intrusion and Freshwater Resources in the Changjiang Estuary. *Journal of Coastal Research*.

MacCready, P. (2011). Calculating estuarine exchange flow using isohaline coordinates. *Journal of Physical Oceanography, 41*(6), 1116-1124.

MacCready, P., Geyer, W. R., & Burchard, H. (2018). Estuarine Exchange Flow Is Related to Mixing through the Salinity Variance Budget. *Journal of Physical Oceanography, 48*(6), 1375-1384. <Go to ISI>://WOS:000437215800010

Monismith, S. G., Kimmerer, W., Burau, J. R., & Stacey, M. T. (2002). Structure and flow-induced variability of the subtidal salinity field in northern San Francisco Bay. *Journal of Physical Oceanography, 32*(11), 3003-3019. <Go to ISI>://WOS:000178834000003

Osborn, T. R., & Cox, C. S. (1972). Oceanic fine structure. *Geophysical Fluid Dynamics, 3*(4), 321-345. <Go to ISI>://INSPEC:439191

Pritchard, D. W. (1956). The dynamic structure of a coastal plain estuary. *Journal of Marine Research, 15*(1), 33-42.

Purkiani, K., Becherer, J., Klingbeil, K., & Burchard, H. (2016). Wind‐induced variability of estuarine circulation in a tidally energetic inlet with curvature. *Journal of Geophysical Research: Oceans, 121*(5), 3261-3277.

Qiu, C., & Zhu, J.-R. (2013). Influence of seasonal runoff regulation by the Three Gorges Reservoir on saltwater intrusion in the Changjiang River Estuary. *Continental Shelf Research, 71*, 16-26. <Go to ISI>://WOS:000329149500002

Qiu, C., Zhu, J., & Gu, Y. (2012). Impact of seasonal tide variation on saltwater intrusion in the Changjiang River estuary. *Chinese Journal of Oceanology and Limnology, 30*(2), 342-351. <Go to ISI>://WOS:000301001900019

Ralston, D. K., & Geyer, W. R. (2019). Response to channel deepening of the salinity intrusion, estuarine circulation, and stratification in an urbanized estuary. *Journal of Geophysical Research: Oceans*.

Ralston, D. K., Talke, S., Geyer, W. R., Al‐Zubaidi, H. A., & Sommerfield, C. K. (2019). Bigger tides, less flooding: Effects of dredging on barotropic dynamics in a highly modified estuary. *Journal of Geophysical Research: Oceans, 124*(1), 196-211.

Stern, M. E. (1968). *T-S gradients on the micro-scale.* Paper presented at the Deep Sea Research and Oceanographic Abstracts.

Wang, T., & Geyer, W. R. (2018). The Balance of Salinity Variance in a Partially Stratified Estuary: Implications for Exchange Flow, Mixing, and Stratification. *Journal of Physical Oceanography, 48*(12), 2887-2899.

Wang, T., Geyer, W. R., & MacCready, P. (2017). Total exchange flow, entrainment, and diffusive salt flux in estuaries. *Journal of Physical Oceanography, 47*(5), 1205-1220.

Wu, H., Gu, J., & Zhu, P. (2018). Winter Counter‐Wind Transport in the Inner Southwestern Yellow Sea. *Journal of Geophysical Research: Oceans, 123*(1), 411-436.

Wu, H., & Zhu, J. (2010). Advection scheme with 3rd high-order spatial interpolation at the middle temporal level and its application to saltwater intrusion in the Changjiang Estuary. *Ocean Modelling, 33*(1-2), 33-51. <Go to ISI>://WOS:000276986700004

Wu, H., Zhu, J., Chen, B., & Chen, Y. (2006). Quantitative relationship of runoff and tide to saltwater spilling over from the North Branch in the Changjiang Estuary: A numerical study. *Estuarine Coastal and Shelf Science, 69*(1-2), 125-132. <Go to ISI>://WOS:000239855300010

Wu, H., Zhu, J., & Choi, B. H. (2010). Links between saltwater intrusion and subtidal circulation in the Changjiang Estuary: A model-guided study. *Continental Shelf Research, 30*(17), 1891-1905.

Wu, H., Zhu, J., Shen, J., & Wang, H. (2011). Tidal modulation on the Changjiang River plume in summer. *Journal of Geophysical Research: Oceans, 116*(C8).

Xue, P., Chen, C., Ding, P., Beardsley, R. C., Lin, H., Ge, J., & Kong, Y. (2009). Saltwater intrusion into the Changjiang River: A model‐guided mechanism study. *Journal of Geophysical Research: Oceans, 114*(C2).

Yang, Y., & Chui, T. F. M. (2018). Combined ecohydrological effects of wind regime change and land reclamation on a tidal marsh in semi-enclosed bay. *Ecological Engineering, 124*, 123-134.

Yang, Z., & Wang, T. (2015). Responses of estuarine circulation and salinity to the loss of intertidal flats–A modeling study. *Continental Shelf Research, 111*, 159-173.

Zhang, E. F., Gao, S., Savenije, H. H. G., Si, C. Y., & Cao, S. (2019). Saline water intrusion in relation to strong winds during winter cold outbreaks: North Branch of the Yangtze Estuary. *Journal of Hydrology, 574*, 1099-1109. <Go to ISI>://WOS:000476962800087

Zhu, J., Ding, P., Zhang, L., Wu, H., & Cao, H. (2006). Influence of the deep waterway project on the Changjiang Estuary. In *The environment in Asia Pacific harbours* (pp. 79-92): Springer.

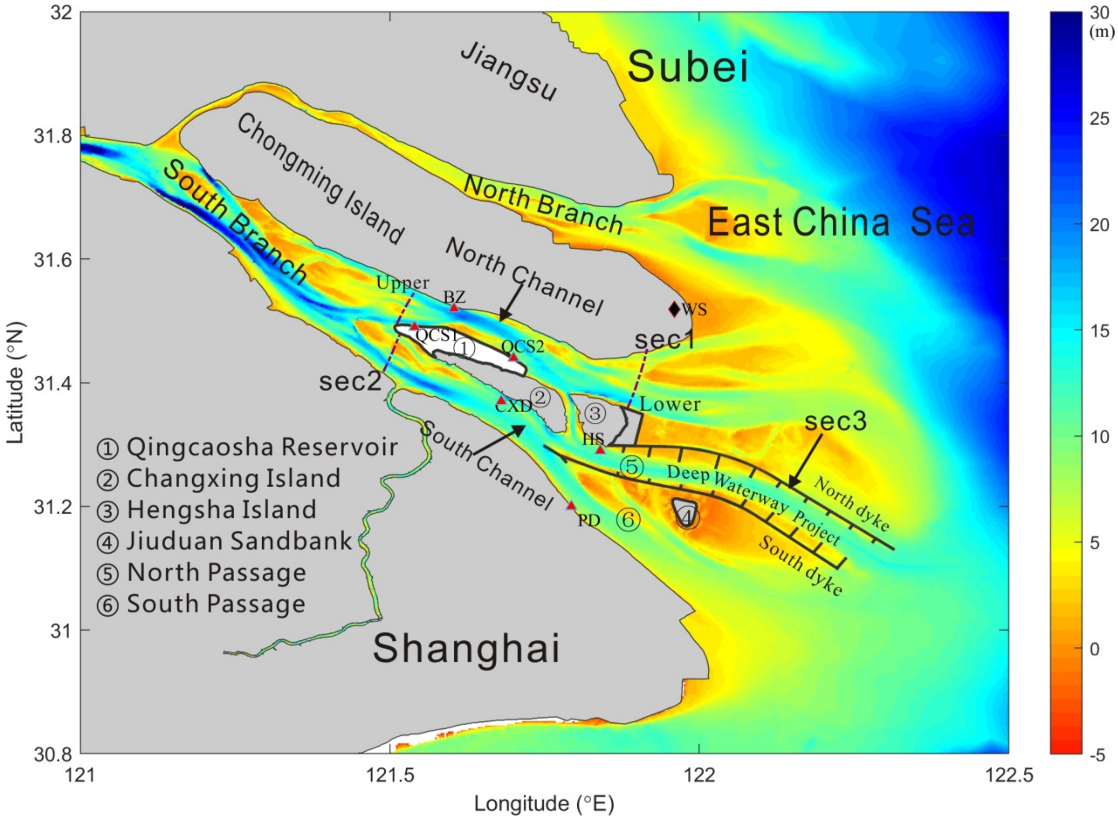

Figure 1. The Changjiang Estuary (bathymetry in colors). Cross-sectionally integrated fluxes are calculated through sections 'sec1', 'sec2', and 'sec3'. Transects labeled 'Lower' and 'Upper' denote the boundaries of a segment for the calculation of salinity variance terms and fluxes. Stations of interest in this study are labeled as follows: BZ (Baozhen), QCS1 (water intake facilities at the Qingcaosha Reservoir), QCS2 (lower Qingcaosha), CXD (Changxing station), HS (Hengsha station), and PD (Pudong Airport station). The weather station here is labeled as WS.

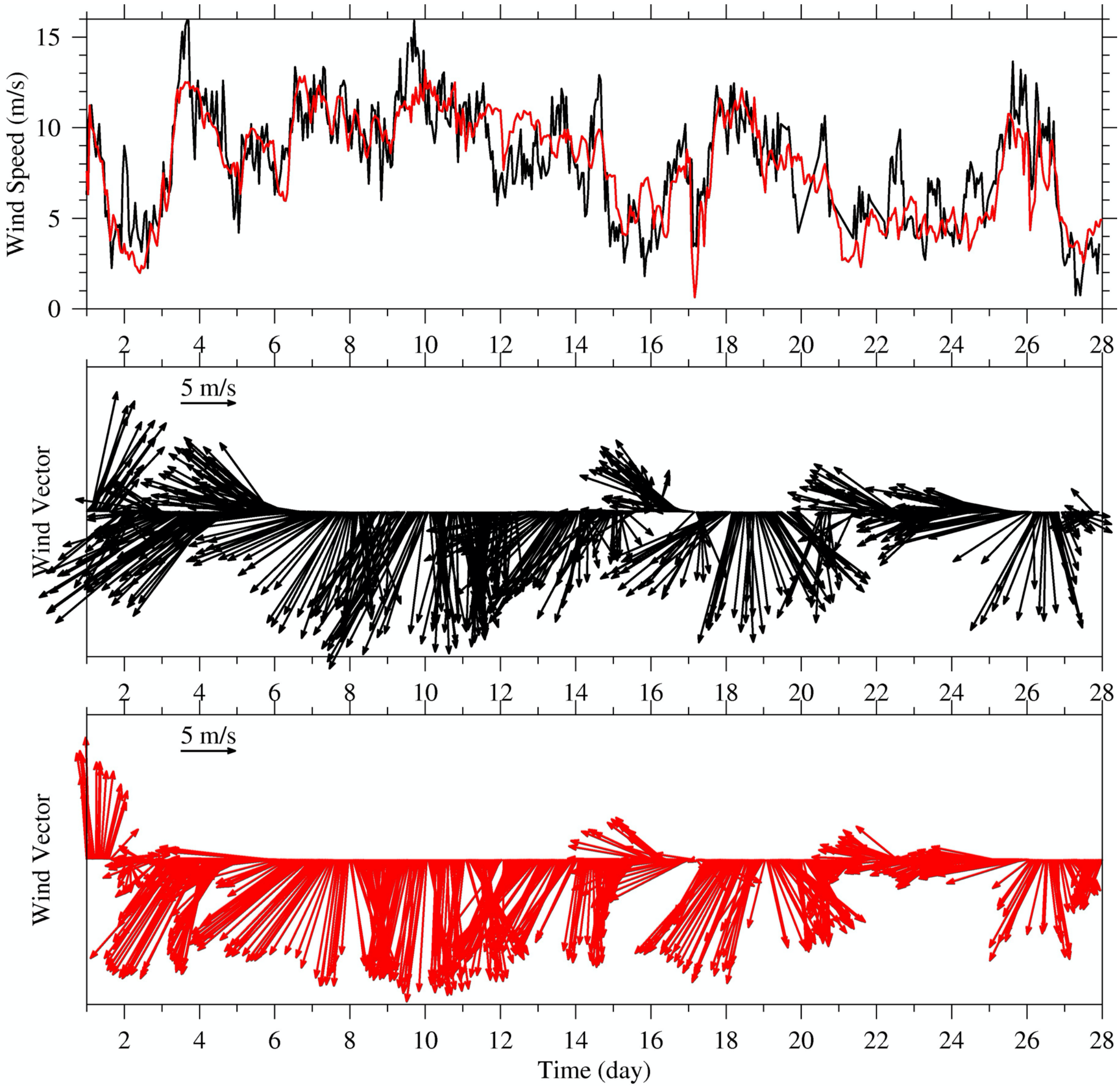

Figure 2. Time series of wind vectors at the east shoal of Chongming Island. (a) Measured (black) and WRF-modeled (red) wind speeds. (b) Measured wind vectors, and (c) modeled wind vectors. The numbers of the x-axis are the date in February, similarly hereinafter.

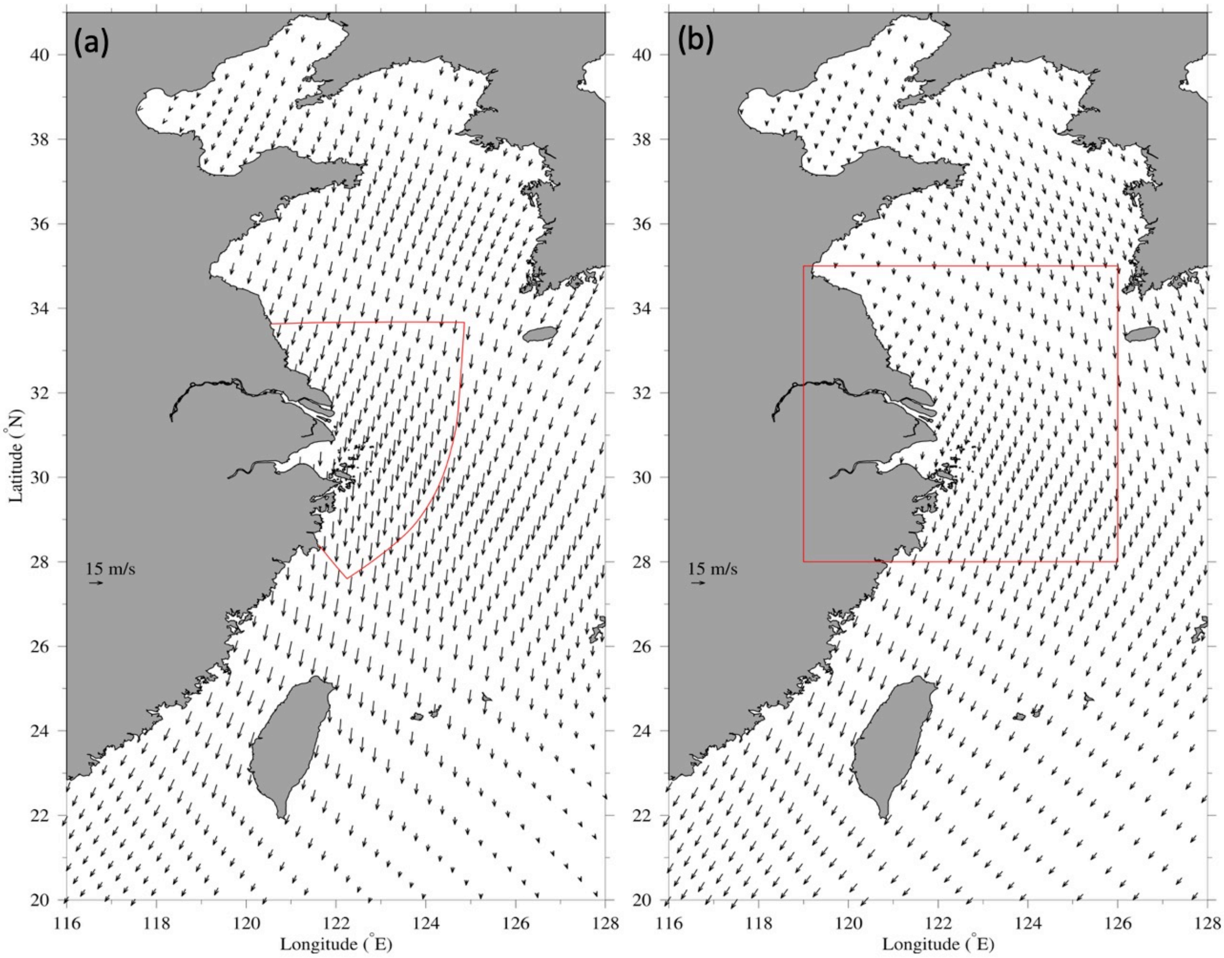

Figure 3. (a) Mean wind field between February 7th and 14th 2014 calculated by the WRF model. (b) Climatic wind field for February. The red line borders (a) the model domain and (b) the area for spatial wind averaging.

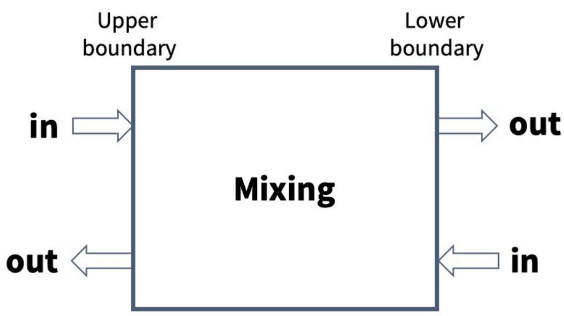

Figure 4. Schematic of an idealized box estuary with salt and water exchange at two boundaries.

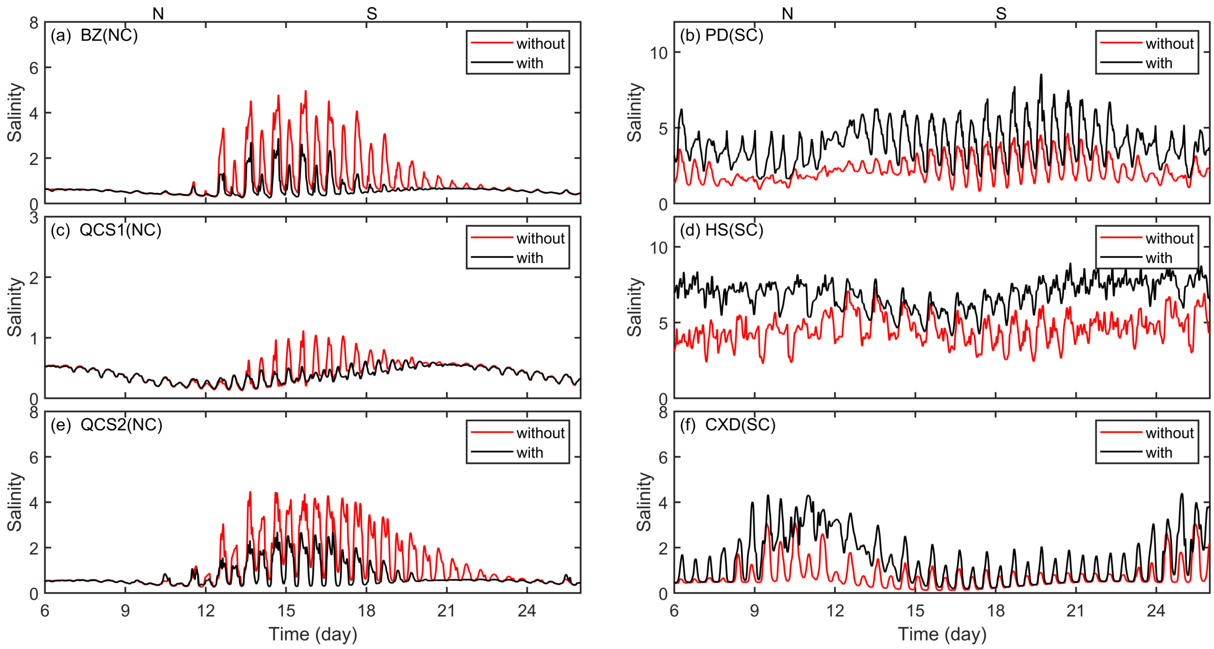

Figure 5. Time series of salinity at the stations in the North Channel (NC, left panel) and in the South Channel (SC, right panel) under climatic wind conditions in February. Times of peak neap and spring tides are marked with ‘‘N’’ and ‘‘S’’ on this and subsequent figures.

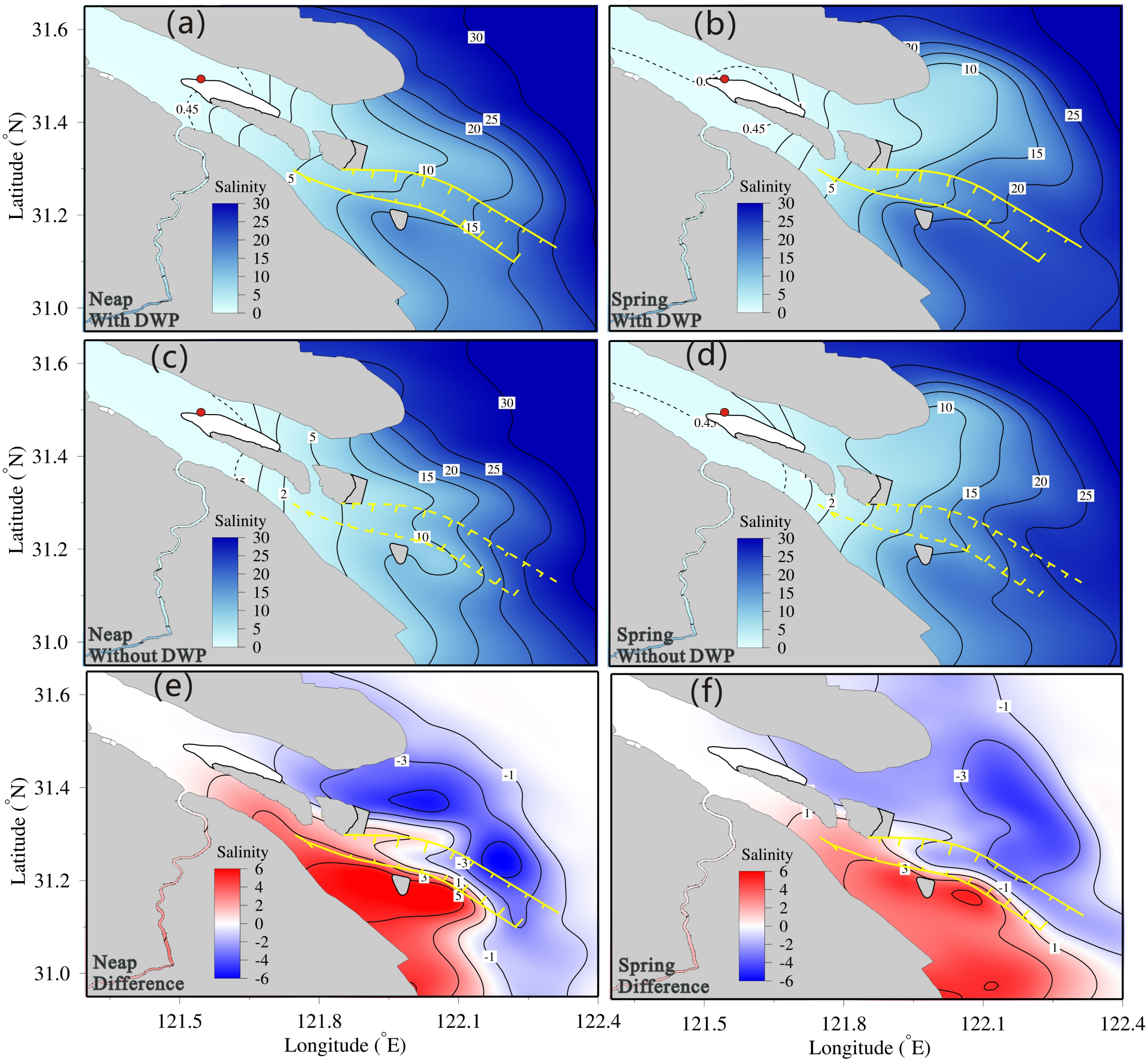

Figure 6. Impact of the DWP on depth-averaged salinity under climatic wind conditions. Neap and spring-averaged fields are shown. (Top row) Scenarios with DWP and (middle row) without DWP. Differences in salinity between scenarios with and without DWP are shown on the bottom row. The dotted contour indicates a salinity of 0.45, which is the standard for drinking water, and the red dot indicates the location of water intake facilities in the Qingcaosha Reservoir.

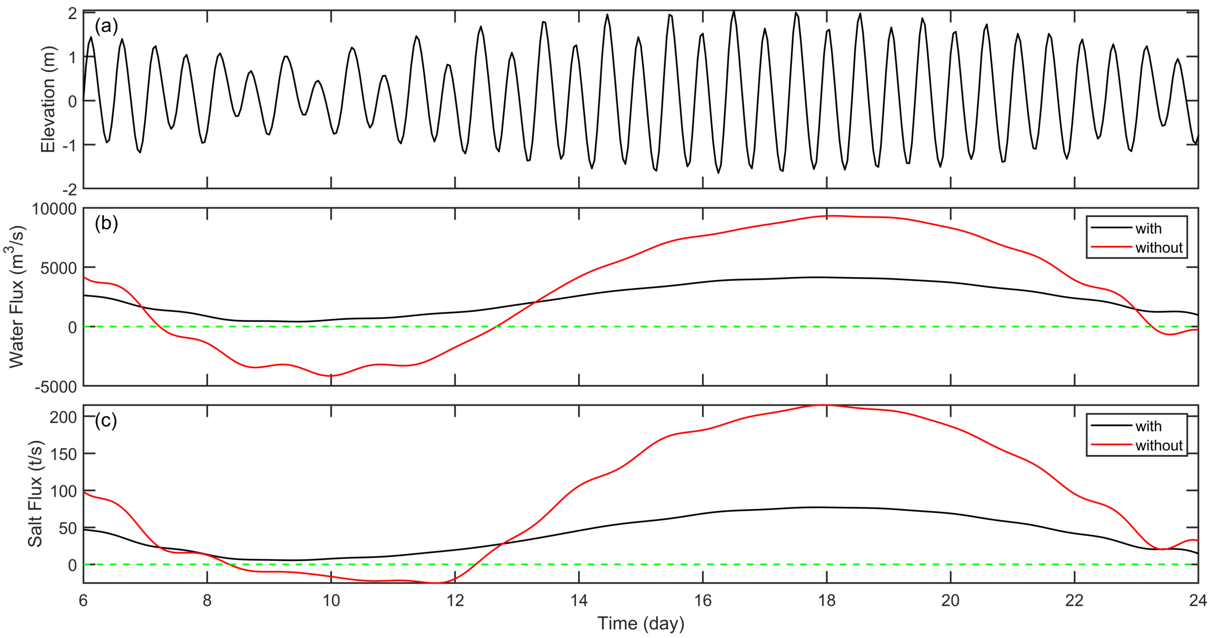

Figure 7. Modeled time series of (a) water level at the Hengsha station, (b) water flux, and (c) salt flux through transect sec3 under climatic wind conditions. Positive and negative values indicate northward and southward, respectively.

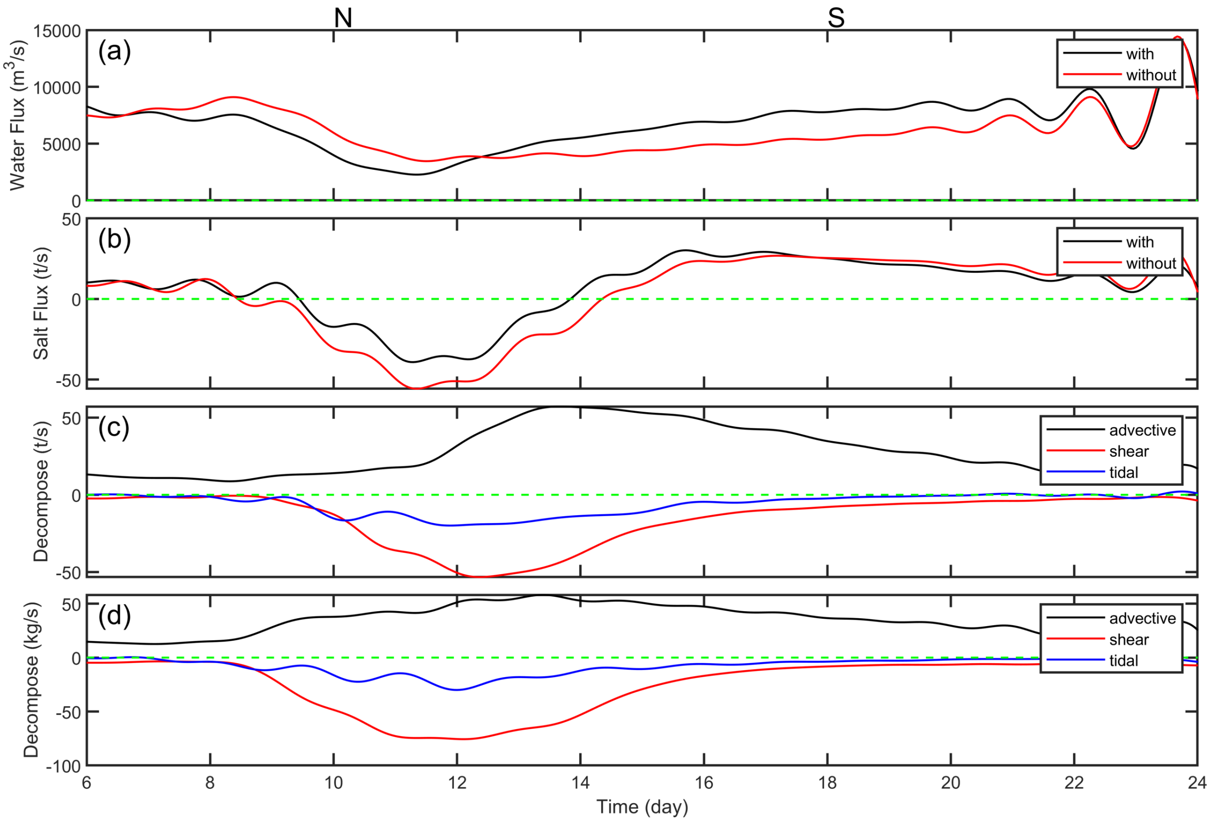

Figure 8. Time series of (a) water fluxes and (b) total salt fluxes in the North Channel (across transect sec1) for scenarios with and without the DWP under climatic winds. Advective, shear, and tidal contributions of the total salt flux are shown in (c) and (d) for scenarios with and without DWP, respectively.

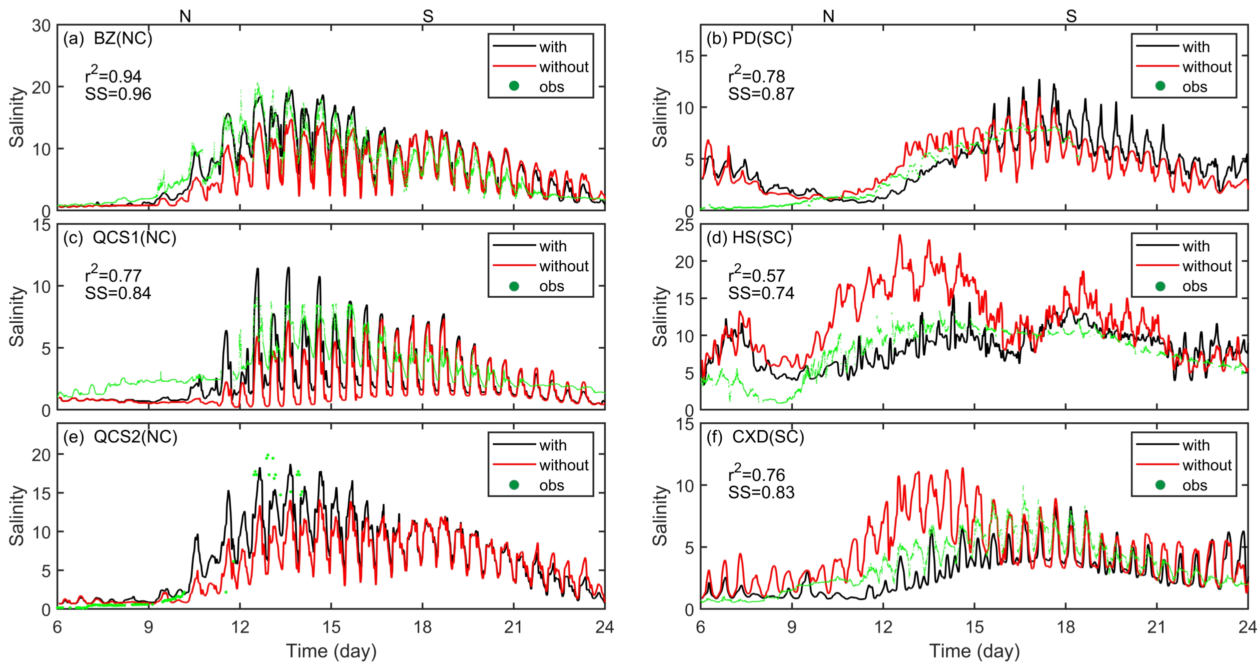

Figure 9. Time series of salinity at stations in the North Channel (left panel) and South Channel (right panel) under the strong, northerly wind conditions of February 2014. Correlation coefficients (r^2) and Skill Scores (SS) are calculated using observations (green) and model results (with DWP, black).

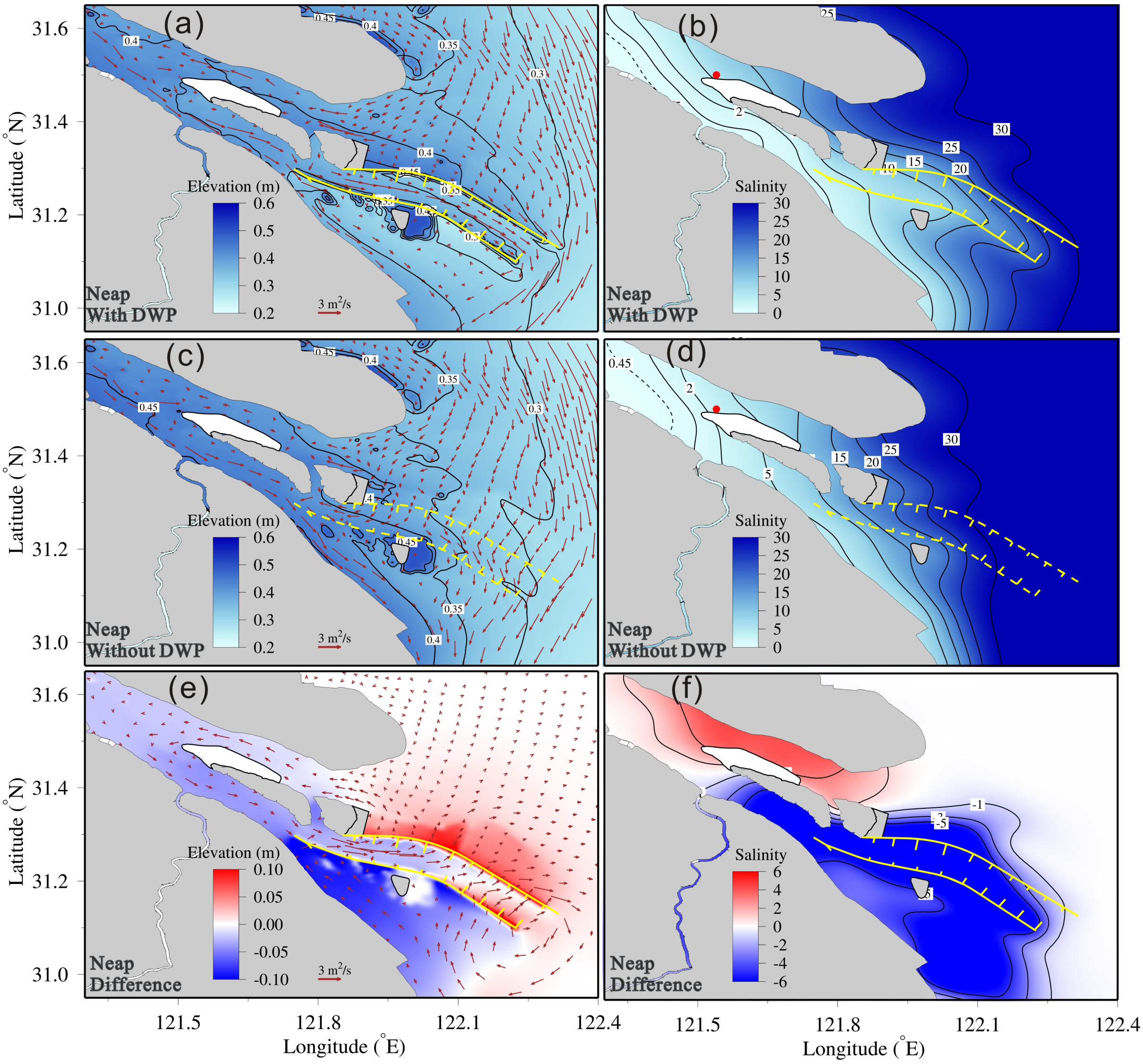

Figure 10. Impact of the DWP on residual elevation, residual water transport, and depth-averaged salinity under strong, persistent winter winds. Averages during neap are shown. Arrows denote residual water fluxes. The residual elevation and water transport are shown in the left column, and the depth-averaged salinity in the right column. Differences between the DWP and no-DWP modeled scenarios are shown in the bottom row.

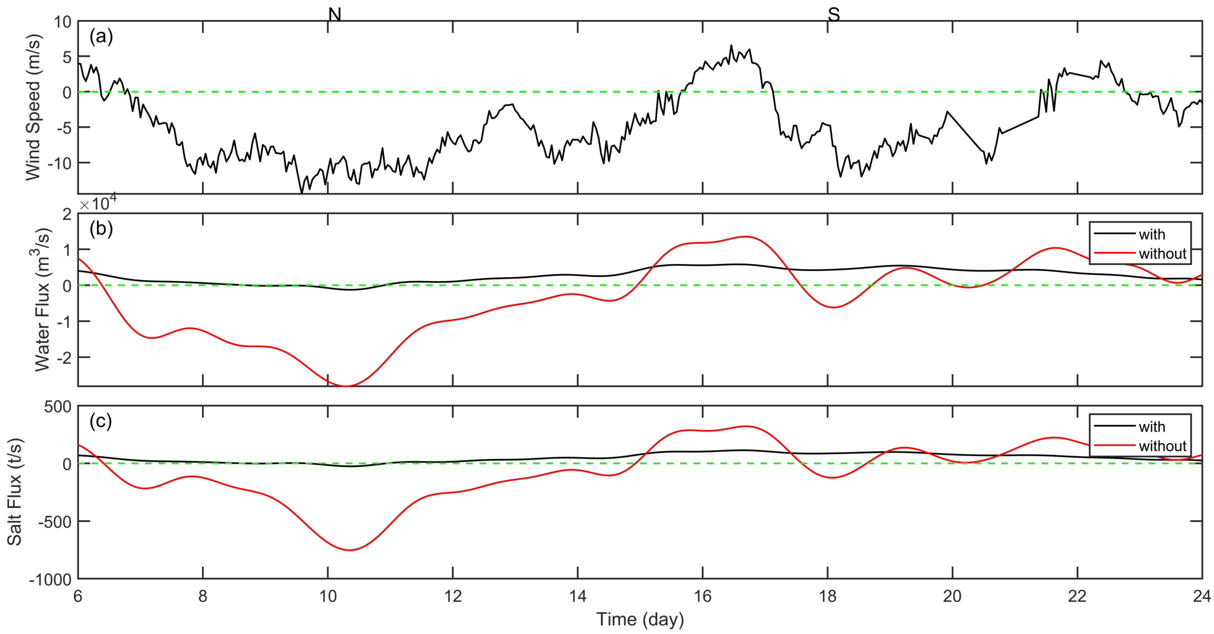

Figure 11. Time series of (a) meridional wind speed, (b) water flux, and (c) salt flux along the north dike under strong, northerly wind in February 2014. Positive values of wind speed correspond to southerly winds, and positive fluxes are northward.

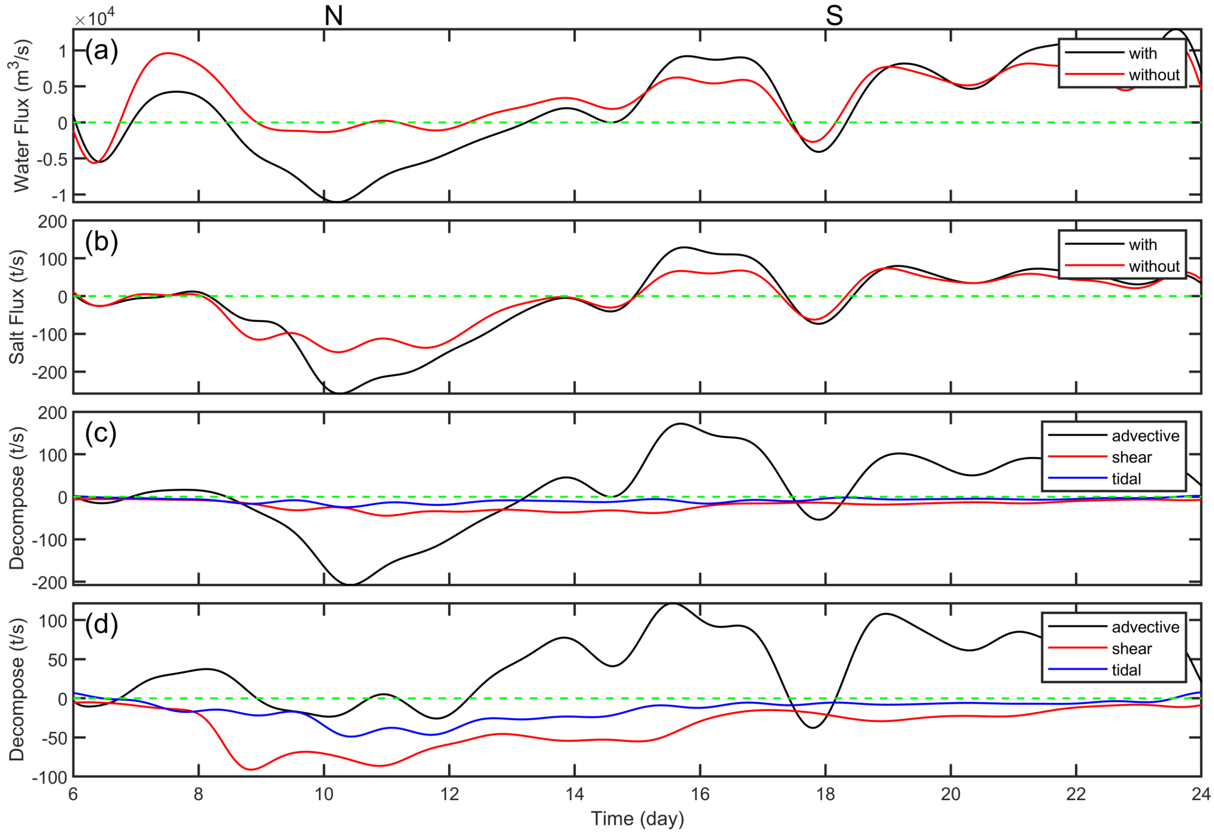

Figure 12. Time series of (a) water fluxes and (b) total salt fluxes in the North Channel (across transect sec1) for scenarios with and without the DWP under the persistent northerly wind conditions in February 2014. Advective, shear, and tidal contributions of the total salt flux are shown in (c) and (d) for scenarios with and without DWP, respectively.

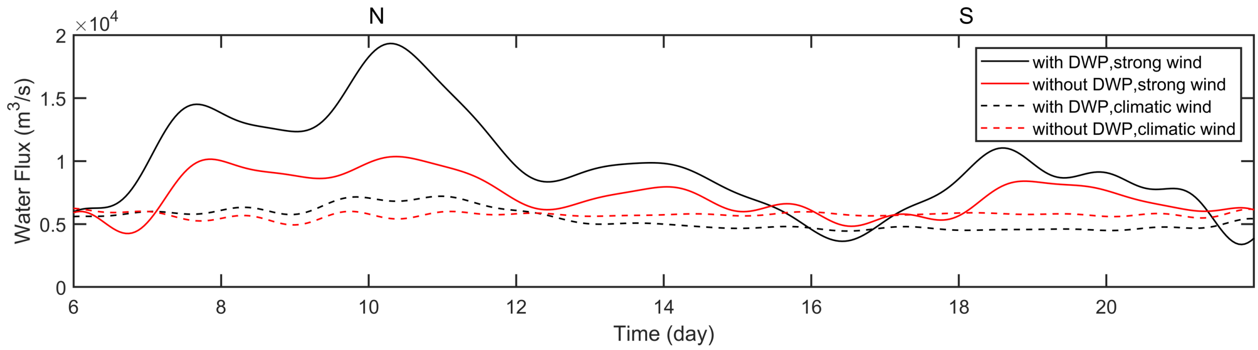

Figure 13. Impact of DWP and wind conditions on water fluxes through the South Channel (sec2). Positive and negative values denote seaward and landward fluxes, respectively.

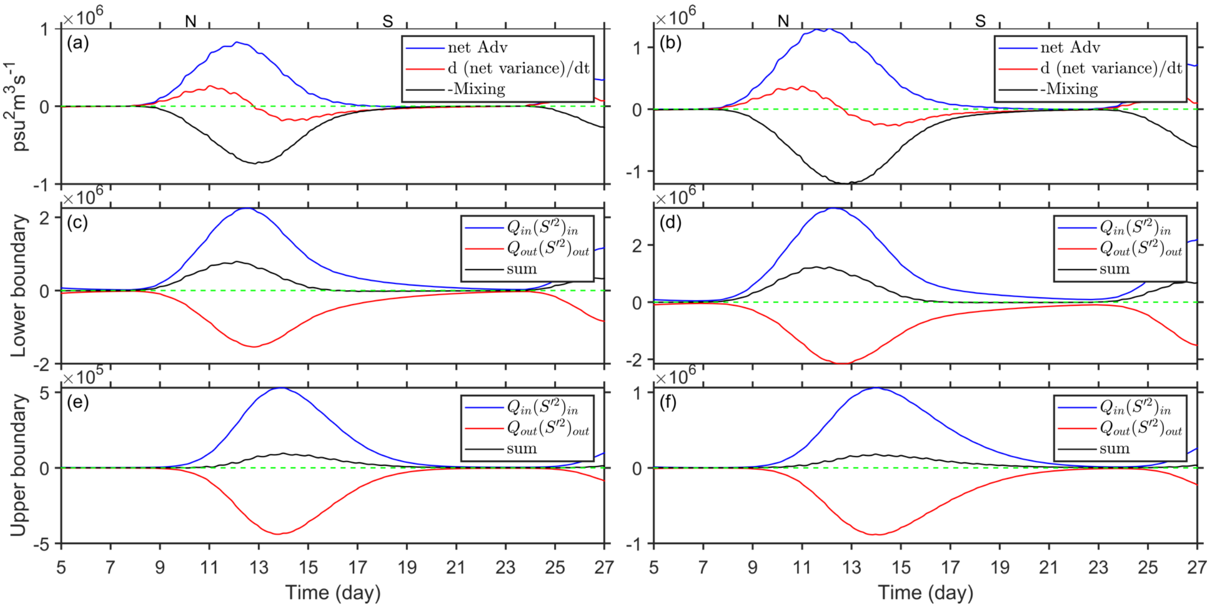

Figure 14. (a) (b) Terms in the salinity variance budget[(13)] under climatic wind conditions , where $d(net\ \text{variance})\ /\ dt\ =\ \dfrac{d}{dt}\left\langle \int S'^2 dV \right\rangle$; $Net\,Adv\ =\ [Q_{in}(S'^2)_{in}\ +\ Q_{out}(S'^2)_{out})\,]\big|_{lower}\ +\ [Q_{in}(S'^2)_{in}\ +\ Q_{out}(S'^2)_{out}\,]\big|_{upper}$; and Mixing=M. (c) (d) The advection of the lower boundary is decomposed into TEF terms as given in (13). $sum\ =\ Q_{in}(S'^2)_{in}\ +\ Q_{out}(S'^2)_{out}$.(e) (f) As in (c) and (d) but at the upper boundary. Left panel shows the results with the implementation of the DWP and right panel shows the results without the implementation of the DWP.

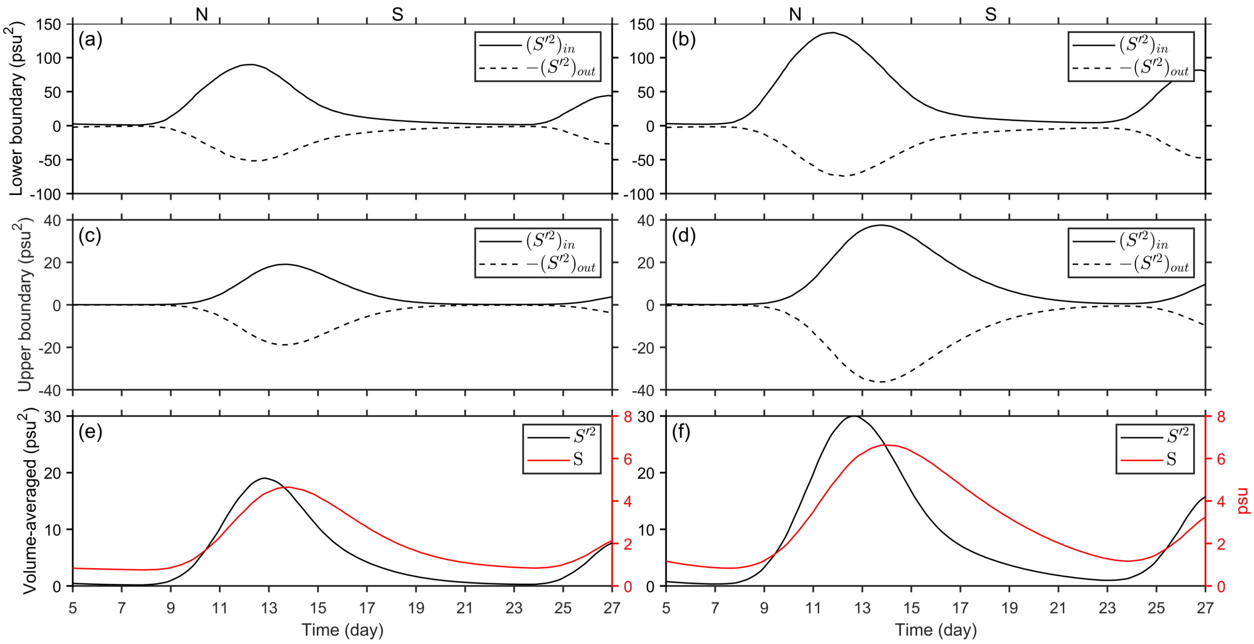

Figure 15. Temporal variations in TEF terms at the boundaries, volume-averaged salinity and salinity variance under climatic wind conditions. The upper panel shows the results at the lower boundary; the middle panel shows the results at the upper boundary; and the lower panel shows the volume-averaged salinity and salinity variance in NC. The left panel shows the results with the implementation of DWP, and the right panel shows the results without the implementation of DWP.

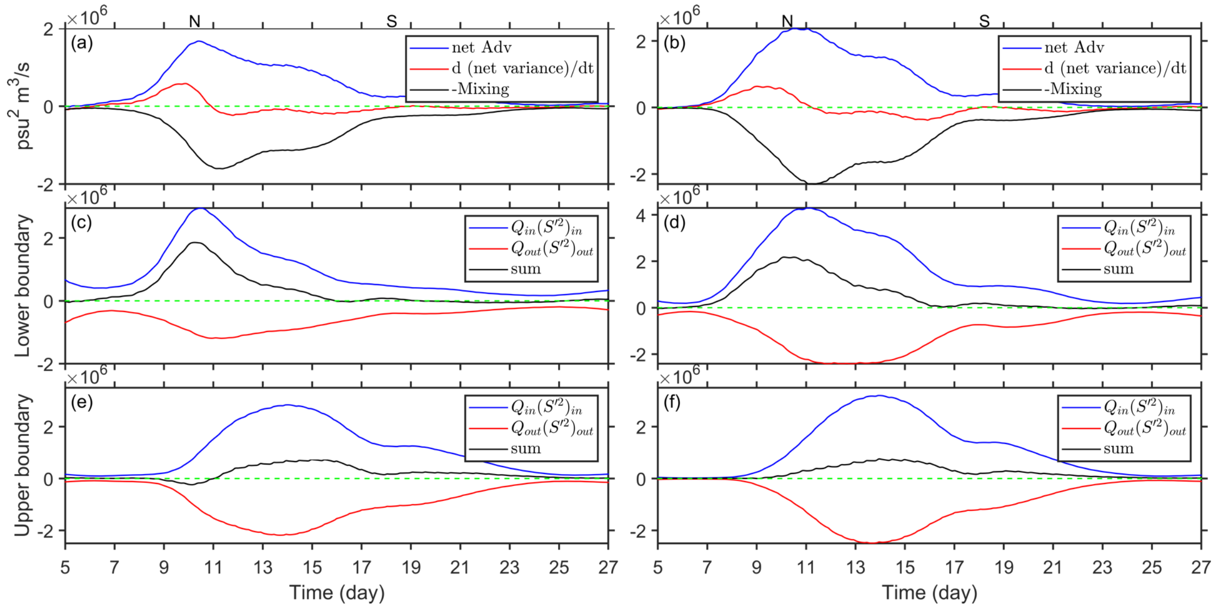

Figure 16. As in Figure 14, but under the strong, northerly wind conditions of February 2014.

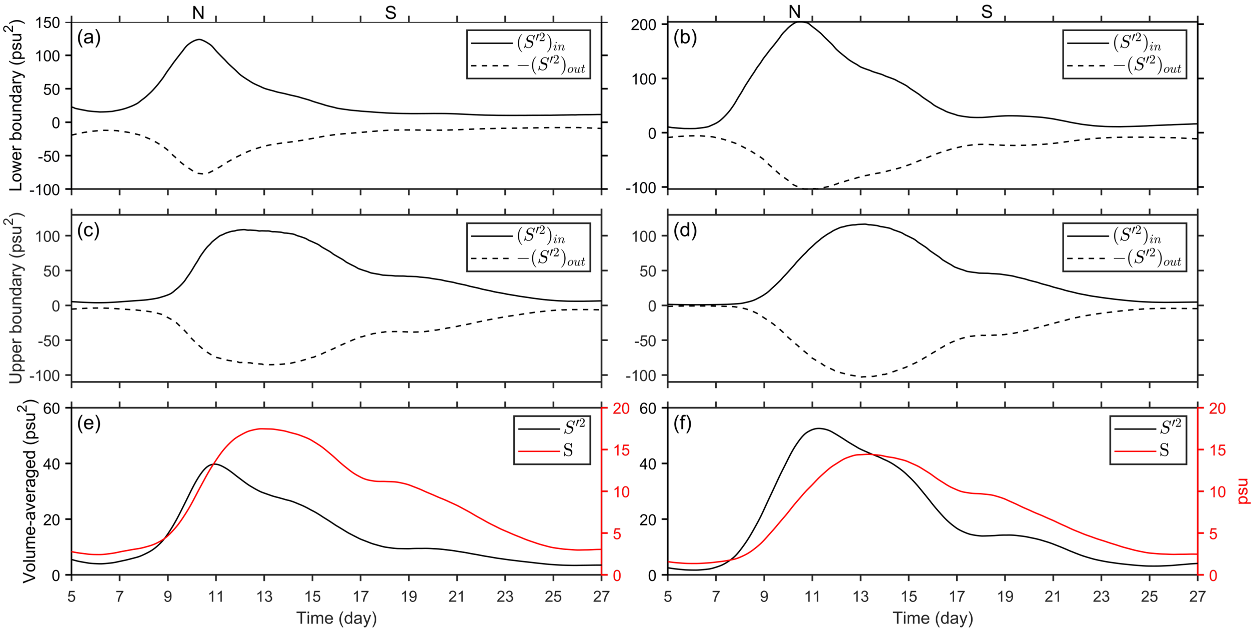

Figure 17. As in Figure 15, but under the strong, northerly wind conditions of February 2014.

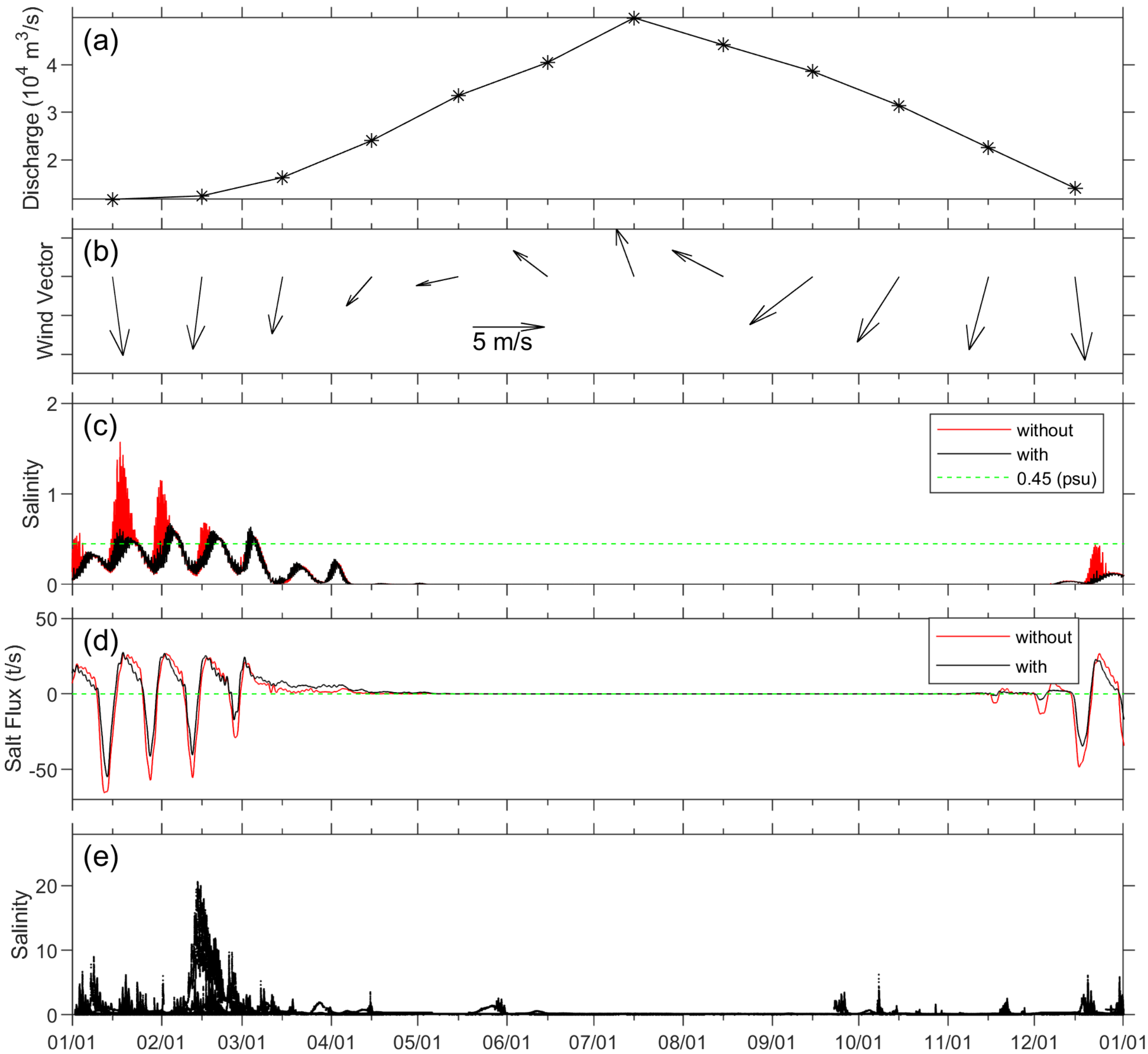

Figure 18. (a) Freshwater discharge climatology at the Datong hydrological station, which are averaged from 1950 to 2019. (b) Monthly mean winds from NCEP/QSCAT, which are averaged over the red box in Figure 3b (c) Salinity at QCS1 (d) Salt flux across sec1, negative means landward. (e) Observed salinity at the BZ station from 2010 to 2018. No distinction is made between years, as we only focus on the seasonal variation.

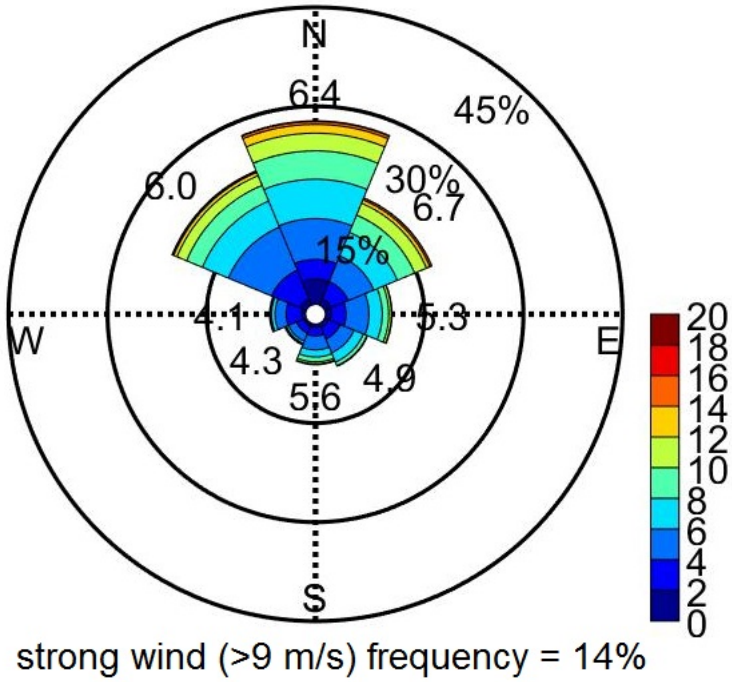

Figure 19. Wind rose for the winter season based on the 2005-2019 period at the WS station. 'N' indicates winds coming from the north.

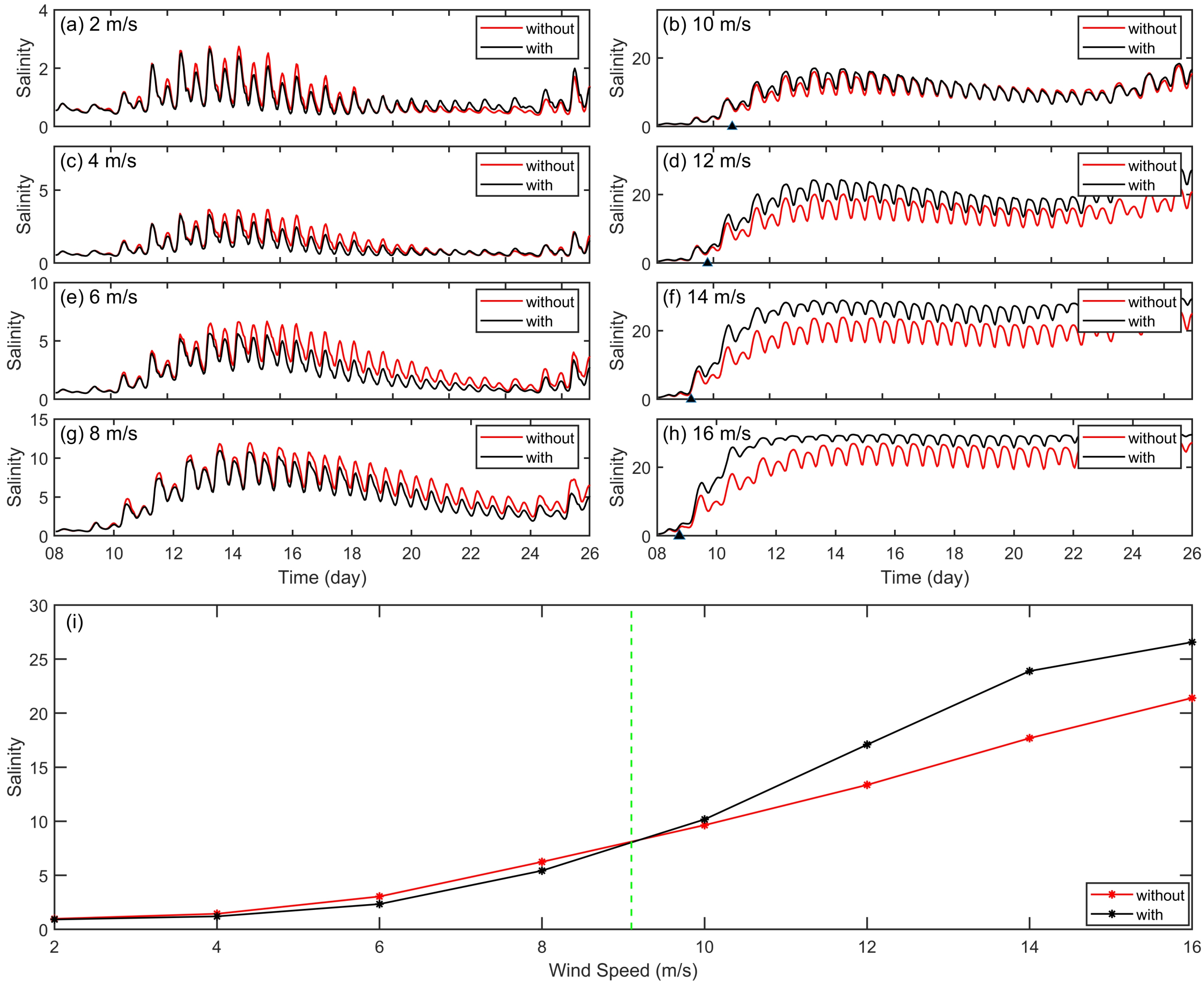

Figure 20. (a)-(h)Time series of volume-averaged salinity of the NC. The black triangles indicate the persistent time for the saltwater intrusion in the NC changing from un-favorable to favorable with the implementation of the DWP. (i) Volume-averaged salinity of the NC, averaged from February 8th to 23rd versus wind speeds.

Table 1. Primary mechanism of landward salt transport across the section in the NC from February 9th to 13th in each scenario.

	with DWP	without DWP
Climatic wind conditions	Steady shear transport	Steady shear transport
Strong winds in February 2014	Advective transport	Steady shear transport

Table 2. Statistics of salinity and salt fluxes in the North Channel during winter season.

	December	January	February	March	Winter season
Number of days with salinity at QCS1 > 0.45	0 (0)	4.3 (8.2)	8.9 (11.8)	2.4 (2.5)	15.6 (22.5)
Maximum salinity at QCS1	0.2 (0.4)	0.6 (1.6)	0.7 (1.2)	0.64 (0.63)	0.7 (1.6)
Mean salinity at QCS1	0.04 (0.06)	0.3 (0.4)	0.35 (0.39)	0.16 (0.16)	0.21 (0.24)
Maximum landward salt flux across sec1	34.5 (48.4)	54.9 (65.4)	40.4 (55.4)	0 (0)	54.9 (65.4)
Mean landward salt flux across sec1	12.6 (20.8)	26.9 (36.7)	18.1 (24.6)	0 (0)	18.9 (27.2)

Note: numbers in brackets indicate scenarios without the implementation of the DWP.